

Accepted Manuscript

Intermolecularly-Induced Conformational Disorder in Ferrocene, 1-Bromoferrocene and 1,1'-Dibromoferrocene

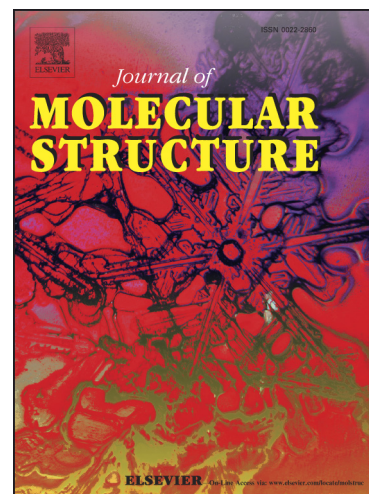
Patrícia A. Silva, Teresa M.R. Maria, Cláudio M. Nunes, Maria Ermelinda S. Eusébio, Rui Fausto

PII: S0022-2860(13)01054-5

DOI: <http://dx.doi.org/10.1016/j.molstruc.2013.12.031>

Reference: MOLSTR 20220

To appear in: *Journal of Molecular Structure*



Please cite this article as: P.A. Silva, T.M.R. Maria, C.M. Nunes, M.E.S. Eusébio, R. Fausto, Intermolecularly-Induced Conformational Disorder in Ferrocene, 1-Bromoferrocene and 1,1'-Dibromoferrocene, *Journal of Molecular Structure* (2013), doi: <http://dx.doi.org/10.1016/j.molstruc.2013.12.031>

This is a PDF file of an unedited manuscript that has been accepted for publication. As a service to our customers we are providing this early version of the manuscript. The manuscript will undergo copyediting, typesetting, and review of the resulting proof before it is published in its final form. Please note that during the production process errors may be discovered which could affect the content, and all legal disclaimers that apply to the journal pertain.

Intermolecularly-Induced Conformational Disorder in Ferrocene, 1-Bromoferrocene and 1,1'-Dibromoferrocene

Patrícia A. Silva, Teresa M. R. Maria, Cláudio M. Nunes,
Maria Ermelinda S. Eusébio and Rui Fausto*

Department of Chemistry, University of Coimbra, P-3004-535 Coimbra (Portugal)

Abstract

Conformational preferences for isolated molecules of ferrocene, 1-bromoferrocene and 1,1'-dibromoferrocene were obtained by combined use of matrix-isolation infrared spectroscopy and quantum chemical calculations. Monomeric ferrocene and 1-dibromoferrocene were found to exist in a low temperature argon matrix ($T = 15$ K) exclusively in the eclipsed configuration, which corresponds to their most stable conformation in gas phase. On the other hand, for the neat compounds in crystalline phase, intermolecular interactions induce conformational disorder, leading to presence in the room temperature polymorphic forms of monomeric units with the staggered (or nearly staggered) conformation. 1,1'-Dibromoferrocene exists in both gas phase and low temperature argon matrix in two conformers of C_2 symmetry (C_{2-I} and C_{2-II}), with eclipsed cyclopentadienyl moieties and Br atoms opposed to H atoms. The populations of the two conformers trapped in the as-deposited matrix were found to correspond to those estimated from theory for the room temperature equilibrium gas phase. By increasing the temperature of the matrix (up to 35 K), the gas phase lower energy form (C_{2-I}) converted to the C_{2-II} form. Besides allowing the precise structural and spectroscopic characterization of the two forms, these studies also revealed that the C_{2-II} conformer (having a largest dipole moment) is stabilized in the matrix media, thus becoming more stable than the C_{2-I} form under these conditions. Very interestingly, the room temperature stable polymorph of the compound ($T_{fus} = 325.4 \pm 0.1$ K) is composed by 1,1'-dibromoferrocene units exhibiting the C_{2v} symmetry eclipsed conformation with opposed bromine atoms, which for the isolated molecule corresponds to the highest energy conformation along the ring torsional coordinate and is the transition state structure between the two symmetry equivalent C_{2-II} minima. Differential scanning calorimetry, polarized light thermomicroscopy and infrared measurements on 1,1'-dibromoferrocene allowed to identify a new polymorph of the compound, with $T_{fus} = 320.2 \pm 0.1$ K. On the whole, the results presented in this article represent illuminating examples of intermolecularly-induced conformational disorder in solid phase and of its relevance to polymorphism.

Keywords: Ferrocene / 1-bromoferrocene / 1,1'-dibromoferrocene / conformational disorder / polymorphism / DFT calculations / matrix isolation IR spectroscopy / DSC / thermomicroscopy.

* Corresponding author e-mail: rfausto@ci.uc.pt

1. Introduction

One of the most important factors responsible for the variety molecular aggregates may exhibit is the similarity between the energies associated with intermolecular nonbonded interactions and those related with intramolecular conformational flexibility ($\sim 1\text{--}40\text{ kJ mol}^{-1}$). Small modifications in the conformation of a molecule can lead to dramatic changes of its properties, including trend to aggregate, reactivity or function. It has been shown, for example, that a specific conformer of *N,N*-dimethylglycine ($\text{N}(\text{CH}_3)_2\text{CH}_2\text{COOH}$) has a greater trend to dimerize than the other experimentally observable conformers of the compound, due to a more favorable charge distribution within the molecule and geometrically more accessible nitrogen lone electron pair and hydroxylic group [1]. On the other hand, a simple molecule like formic acid (HCOOH) has been shown to photochemically react upon UV excitation through different preferred channels, depending of the initial conformation, with the *cis* conformer being transformed preferentially into $\text{H}_2 + \text{CO}_2$ and the *trans* form into $\text{H}_2\text{O} + \text{CO}$ [2]. In biochemistry, molecular conformations largely determine, for instance, catalytic mechanisms in enzymes, antifreeze cryoprotectants efficiency and membrane properties, and are the basis of the general phenomenon of molecular recognition. Conformational changes are key events in the vision process [3], in the control of membrane permeability and molecular transport in cells [4], and in many biosynthetic mechanisms, including that of ATP [5]. Protein folding is also controlled by the conformations of the constituting amino acids. In all these cases, a subtle balance between the intramolecular conformational preferences and the involved intermolecular nonbonded interactions plays a decisive role.

In the chemistry and physics of the organic solid state, conformationally flexible molecules are usually prone to polymorphism [6-9]. In typical cases, different conformations may lead to different polymorphs, where a less favorable conformational arrangement might be compensated by a more stabilizing intermolecular packing [7,10-14]. Alternatively, different molecular conformations might be simultaneously present in the same crystal [6,14-16].

In general, the molecules which are present in the crystals assume conformations resembling those corresponding to possible minimum energy configurations for the isolated molecule, *i.e.*, the conformational order characteristic of the gas phase is approximately kept in the crystal. Profound changes in the typical conformational order of the isolated molecule upon crystallization are much less frequent, since they require a rather efficient packing to compensate the energetic demand resulting from unfavorable conformational intramolecular arrangements.

On the other hand, for very conformationally flexible systems, the molecules may exhibit large amplitude vibrations along the soft torsional coordinates even in the crystalline state. In these cases, structural methods like static X-ray diffraction cannot precisely determine the

conformations assumed by the molecules in the crystal. The expression conformational disorder is currently used also to refer to this situation, even though it is possible that in many cases the large amplitude torsional movements roughly obey the potential energy profile characteristic of the isolated molecule.

In the present article, we will present enlightening examples of intermolecularly-induced conformational disorder, either taken as a strong perturbation of the conformational landscape of the isolated molecule due to intermolecular forces or as a significant statistical uncertainty due to existence of large amplitude torsional movements in the crystal. The systems investigated are ferrocene and its 1-bromo and 1,1'-dibromo derivatives. Firstly, one will show that all these three molecules exist both in the gas phase and in a cryogenic inert matrix in well-defined conformers, whose structures and infrared spectra can be unequivocally established. Then, the conformations assumed by the molecules of the compounds in different polymorphic forms will be compared with those characteristic of the isolated molecules. As it will be shown in detail, isolated ferrocene and 1-dibromoferrocene molecules were found to exist exclusively in the eclipsed conformation in the low temperature matrices, while in crystalline phase intermolecular interactions induce conformational disorder, leading to presence in the room temperature polymorphic forms of monomeric units with the staggered (or nearly staggered) conformation. On the other hand, isolated 1,1'-dibromoferrocene monomer exists as a mixture of two eclipsed conformers in which the Br atoms oppose to H atoms, whereas the room temperature stable polymorph of the compound is composed of molecular units exhibiting the eclipsed conformation with opposed Br atoms, which for the isolated molecule corresponds to the highest energy conformation along the ring torsional coordinate. The conformations of the molecules in the low temperature polymorphs of ferrocene and 1,1'-dibromoferrocene (this one identified in this study for the first time) are also discussed at light of conformational order/disorder.

2. Experimental and Computational Methods

2.1. Matrix-isolation and low temperature FTIR spectroscopy experiments. Ferrocene and their studied bromo-derivatives (1-bromoferrocene and 1,1'-dibromoferrocene) were kindly provided by Professor Luís M. N. B. F. Santos (Centro de Investigação em Química, Department of Chemistry, Faculty of Science, University of Porto). The compounds were purified by sublimation at reduced pressure and their purity (>99.99%) determined by gas chromatography.

The low temperature matrices were produced by co-deposition of the vapor of the ferrocene under study with argon (N60, supplied by Air Liquide) at a molar ratio of ~1:1000 onto a CsI substrate cooled to 15 K. The ferrocenes were sublimated from a specially designed doubly thermostatable Knudsen cell with shut-off possibility (whose main component is a

NUPRO SS-4BMRG needle valve) assembled to the cryostat (APD Cryogenics closed-cycle helium refrigeration system, with a DE-202A expander). The low temperature neat amorphous film of ferrocene was prepared in a similar way. The temperature was directly measured at the sample holder by a silicon diode sensor connected to a digital controller (Scientific Instruments, Model 9650-1), with an accuracy of 0.1 K.

The infrared spectra of the matrix-isolated compounds and low temperature neat solid film of ferrocene were recorded with a resolution of 0.5 cm^{-1} , using a Thermo Nicolet 6700 Fourier-transform infrared (FTIR) spectrometer, equipped with a KBr beam splitter and a deuterated triglycine sulfate (DTGS) detector. In the temperature variation infrared studies performed for the compounds diluted in a KBr pellet the same spectra recording conditions were used for low temperature measurements, while a Specac variable temperature cell and resolution 1 cm^{-1} were used for studies above room temperature. In all cases, the sample compartment of the spectrometer was purged by means of a constant flux of dry nitrogen, to avoid contamination from absorptions due to atmospheric water and CO_2 .

2.2. Differential scanning calorimetry (DSC) and polarized-light thermomicroscopy (PLTM) studies. Thermal studies were carried out in a Perkin Elmer DSC7 differential scanning calorimeter, with an intracooler cooling unit at 263 K (ethylenglycol-water 1:1 v/v cooling mixture), with scanning rates $2\text{-}10\text{ K min}^{-1}$ over a temperature range from 285 K to the melting point of each compound. Data acquisition and determination of the onset temperatures and transition enthalpies were performed with Pyris software version 3.5. The samples were hermetically sealed in aluminium pans and an empty pan was used as reference. No sample weight loss occurred in any experiment. A 20 mL min^{-1} nitrogen purge was employed. Temperature calibration [17] was performed with high grade standards, namely benzophenone (Mettler Toledo Calibration substance, $T_{\text{fus}} = 321.3 \pm 0.2\text{ K}$) and indium (Perkin-Elmer, $x = 99.99\%$, $T_{\text{fus}} = 429.75\text{ K}$). For heat calibration, the enthalpy of fusion of indium was used ($\Delta_{\text{fus}}H = 3286 \pm 13\text{ J mol}^{-1}$) [17]. The numerical values presented in this study for phase transition temperatures and enthalpy changes are the mean of $n \geq 4$ independent experiments, with the uncertainties expressed as one standard deviation.

The hot stage/DSC video microscopy study was carried out by means of a Linkam DSC600 system. The optical equipment attached to the hot stage system consists of a DMRB Leica microscope fitted with polarized light facilities, to which a Sony CCD-IRIS/RGB video camera is attached. A Linkam system software with Real Time Video Measurement was used for image analysis. A small amount of the sample to be studied was placed in a glass crucible used as a cell, which was covered with a glass lid. Thermal cycles were followed by 200x magnification and the images obtained by combined use of polarized light and wave compensators. The thermal program for the microscope examination was run at 10 K min^{-1} . Biphenyl and benzoic acid were used to confirm temperature accuracy.

2.3. Theoretical calculations. All theoretical calculations were performed using Gaussian 03 [18], at the DFT/B3LYP level of theory [19], with the cc-pVDZ basis set for C, H and Br atoms and the LANL2DZ (Los Alamos National Laboratory 2 double- ζ) effective core potential (ECP) on the transition metal [20-22]. According to previous theoretical studies on ferrocene [23,24], the B3LYP functional was found to reproduce adequately the structure of the compound, while the LANL2DZ ECP-type basis set has been receiving wide successful applications to model metal atoms [22,24,25]. The nature of the stationary points obtained upon geometry optimization was checked by analysis of the corresponding Hessian matrix. For the purpose of modeling IR spectra, the calculated frequencies, together with the calculated IR intensities, served to simulate the spectra shown in the figures by convoluting each peak with a Lorentzian function with a proper full width at half-maximum (FWHM) (2 cm^{-1} in case of simulation of matrix isolation spectra and $5\text{-}10\text{ cm}^{-1}$ in case of neat solid samples' spectra). Assignment of vibrational modes was done with help of the animation module of Chemcraft (version 1.6) [26].

3. Results and Discussion

3.1. Theoretical investigation of the structural preferences for the isolated molecules.

The conformational study of ferrocene, 1-bromoferrocene and 1,1'-dibromoferrocene was performed at the DFT/B3LYP level of theory, with the cc-pVDZ basis set for C, H and Br atoms and the LANL2DZ (Los Alamos National Laboratory 2 double- ζ) ECP on the transition metal. Figure 1 shows the calculated potential energy profiles obtained for the 3 molecules resulting from varying the relative orientation of the two rings. Table 1 summarizes the energetic data for the minimum energy structures and transition states.

Both ferrocene and 1-bromoferrocene present a five-fold potential energy profile along the chosen driving coordinate, with minima at the eclipsed (D_{5h} symmetry for ferrocene) conformations. The staggered conformations (D_{5d} symmetry for ferrocene) correspond to transition states, their B3LYP/LANL2DZ + cc-pVDZ calculated energies being *ca.* 1.9 kJ mol^{-1} above those of the eclipsed forms in both molecules. In case of the parent ferrocene, the minimum energy conformation in the gas phase has been determined long ago by electron diffraction [27,28], and shown to be the eclipsed form, the barrier to internal rotation being $3.8 \pm 1.3\text{ kJ mol}^{-1}$. Previously reported values for this energy barrier, calculated at different levels of theory, are in the range $0.3\text{-}19.1\text{ kJ mol}^{-1}$ [23,29], indicating the sensitivity of this property to the used theoretical model. In all cases, however, the theoretical approaches predict the eclipsed conformation as being the minimum energy structure for the isolated molecule and the staggered one as the transition state. In view of the available data, one can conclude that the

present calculations slightly underestimate the rotation barrier in ferrocene, and probably also in 1-bromoferrocene by a similar amount (for this molecule, no internal rotation barrier has been reported hitherto, either experimental or theoretically). Nevertheless, the present calculations indicate that the barriers in the two molecules are, almost certainly, identical. The gas phase equilibrium conformation of 1-bromoferrocene has also been shown to be the eclipsed form through analysis of its rotational spectrum by microwave spectroscopy [30].

The B3LYP/LANL2DZ + cc-pVDZ calculated internal rotation profile for 1,1'-dibromoferrocene is rather more complex than for both the unsubstituted ferrocene and 1-bromoferrocene. As shown in Figure 1, the molecule has two different two-fold minima of C_2 symmetry, with eclipsed rings and Br atoms opposed to H atoms: C_2 -I, where the planes containing the two C–Br and opposed C–H bonds define a dihedral of 144° , and C_2 -II, where this dihedral is 72° . The C_2 -I conformer is predicted to be more stable than C_2 -II by 0.82 kJ mol^{-1} , and the barrier of energy between the two forms, at the intermediate staggered conformation, to be 1.38 kJ mol^{-1} (0.56 kJ mol^{-1} in the C_2 -II \rightarrow C_2 -I direction). At room temperature, the calculated Gibbs energy difference (ΔG) between the two conformers amounts to 1.25 kJ mol^{-1} , which leads to predicted Boltzmann populations for the two conformers in the gas phase room temperature equilibrium of 62% (C_2 -I) and 38% (C_2 -II).

The C_{2h} symmetry staggered and C_{2v} symmetry eclipsed conformations of the molecule of 1,1'-dibromoferrocene correspond to the transition states between the two-symmetry equivalent C_2 -I and the two symmetry equivalent C_2 -II forms, respectively, and define barriers for interconversion between these forms equal to 1.66 and 4.91 kJ mol^{-1} . It shall be highlighted here that the C_{2v} eclipsed conformation is, along the ring torsional coordinate, the highest energy configuration in isolated 1,1'-dibromoferrocene.

Table 2 shows the calculated average relevant geometrical parameters for minima and transition state structures of the 3 studied molecules. The full optimized geometries are provided in Table S1 (Supporting Information). The obtained structures for both ferrocene and 1-bromoferrocene agree rather well with the experimental data, in particular for the first molecule, for which equilibrium (r_e) experimental parameters are available (for 1-bromoferrocene the agreement is not so good because the considerable number of assumed geometrical parameters and absence of vibrational corrections in the experimental work [30]; see Table 2). It shall, however, be noticed that the theoretically obtained Fe–C and C–Br distances are somewhat longer than the experimental ones. As detailed in the next section, in the case of the Fe–C distances this fact has a relevant implication for the performed vibrational calculations, since contrarily to the general rule the calculated frequencies for modes with predominant contribution of this coordinate are slightly underestimated. Another general conclusion that can be extracted from the structural data is that for the same molecule, the changes in conformation do not lead to significant variations in the geometrical parameters, the

largest differences being observed for the C_{2v} form of 1,1'-dibromoferrocene due to the close proximity of the two Br atoms in this structure. Furthermore, identical parameters in different molecules are also predicted by the calculations to assume very similar average values, indicating that the presence of the bromine atoms does not considerably perturb the molecular structure. Nevertheless, a detailed analysis of the individual structural parameters in 1-bromo and 1,1'-dibromoferrocene molecules shows that both the Fe–C(Br) and C–C(Br) distances are slightly shorter (by ca. 0.013 and 0.001 Å, respectively) than the remaining Fe–C(Br) and C–C(Br) distances in the minimum energy structures.

3.2. Experimental studies.

3.2.1. **Ferrocene.** The structure of ferrocene was first investigated in its room temperature crystalline state by X-ray diffraction by 3 independent groups [31-33]. In these pioneer studies the staggered D_{5d} structure was proposed as corresponding to the species existing in the crystal, because it was considered to be the unique compatible with the molecular inversion centre required by the space group ($P2_1/a$, $Z = 2$; monoclinic). However, the posterior analysis of the 3D structure of the crystal [34] showed that a considerable smearing of the electron-density maxima occurs in the planes of the cyclopentadienyl rings, while thermodynamic studies indicated that ferrocene has a λ -transition at ca. 169 K that is accompanied by an increase of entropy of $\sim 5 \text{ J K}^{-1} \text{ mol}^{-1}$ on heating [35]. These data revealed that a considerable degree of disorder should be associated with the higher-temperature phase. Occurrence of disorder in room temperature crystalline ferrocene was also indicated by neutron diffraction studies [36]. In the presence of disorder associated with the relative orientation of the two cyclopentadienyl rings, the requirement for a centrosymmetric form of individual molecules of ferrocene in the room temperature crystalline phase breaks, and models were then proposed where molecules with different conformations were considered to be present in the crystal [36-39]. Two main discoveries stimulated the new interpretations for the structure of the room temperature crystalline phase of ferrocene. Firstly, as already mentioned, the experimental determination by electron diffraction that the equilibrium geometry of ferrocene in the gas phase is the eclipsed one (D_{5h}) [27,28]. Secondly, the 3D structure determination of the second polymorph of ferrocene ($F\bar{1}$, $Z = 16$; triclinic), which showed that in this polymorph the molecules assume a conformation deviated only 9° from the eclipsed form [40].

Very interestingly, the precise structure of the monoclinic room temperature crystalline phase of ferrocene is still controversial [38,39], though there is a general agreement that it is characterized by a considerable degree of disorder and that the crystallographic “evidence“ for the staggered arrangement of the cyclopentadienyl rings is only statistic in nature. The onset of disorder at the λ -transition appears to be determined by the loss of the long-range order present in the low temperature triclinic polymorph upon conversion to the monoclinic phase, much

probably induced by the gradual increase with temperature of the amplitude of the vibration along the cyclopentadienyl torsional coordinate [38]. However, occurrence of static disorder due to simultaneous presence of an increasing number of molecules in other than the eclipsed conformation has also been proposed to justify the experimental findings [38,39].

More recently, more data have been reported supporting the prevalence of the eclipsed or nearly eclipsed conformations of ferrocene. First of all, the discovery of a third polymorph of the compound (*Pnma*, $Z = 4$; orthorhombic; the thermodynamically stable polymorph at temperatures below *ca.* 242 K), where the equilibrium configuration of the molecules is *exactly* eclipsed [41-44]. Later on, the confirmation by quantum chemical theoretical methods that the equilibrium geometry of the isolated molecule of ferrocene shall indeed be the eclipsed one [23,24,29]. Finally, the recent indication from a combined infrared and theoretical study that the eclipsed conformation of ferrocene also dominates in solution of non-polar solvents [45].

In the experimental study described in the present report, we started by recording the infrared spectrum of ferrocene monomer isolated in a low temperature argon matrix. This methodology was chosen because it could be expected to provide the pure vibrational spectrum of the molecule of ferrocene in its preferred conformation with a high-spectral resolution and without the complexity associated to the characteristic rotational structure of a gas-phase infrared spectrum [46]. In fact, under matrix isolation conditions (very low work temperature – in this case, 15 K –, and absence of molecular diffusion, rotation and strong interactions with the environment), the comparison between experimental spectra and those obtained theoretically is facilitated, allowing for identification of fine structural details of the studied molecule.

The infrared spectrum (3200-450 cm^{-1} region) of matrix-isolated ferrocene is shown in Figure 2, together with the B3LYP/LANL2DZ + cc-pVDZ calculated spectrum for the D_{5h} minimum energy structure of the compound. Note that due to the symmetry of the molecule only a few modes are active in infrared (the A_2'' and E_1' type vibrations), corresponding to just 9 bands in the studied spectral region. The proposed assignments are presented in Table 3. The full calculated spectra for both D_{5h} and D_{5d} conformations are provided in Table S2 (Supporting Information).

The first point to note here is the fact that the infrared spectra predicted for different conformations of ferrocene (differing in the relative orientation of the cyclopentadienyl rings) are rather similar. However, as noticed before [29,45], the infrared spectral region between 450 and 530 cm^{-1} is a conformationally sensitive region and can be used to differentiate the possible molecular structures. As shown in Figure 3, in the D_{5h} conformation, the E_1' Cp-Fe wagging mode is predicted at 500 cm^{-1} and the A_2'' mode (Cp-Fe “top-down” vibration) at 484 cm^{-1} ($\Delta\nu = \nu E_1' - \nu A_2'' = 16 \text{ cm}^{-1}$), the first mode decreasing its frequency with the increase of the torsion angle between the two rings and the second varying in such a way that for the D_{5d} conformation the two modes almost coincide. The B3LYP/LANL2DZ + cc-pVDZ calculated

$I^{\text{IR}}(E_1')/I^{\text{IR}}(A_2'')$ intensity ratio is 3.9 for the D_{5h} minimum energy conformation, while the ratio between the intensity of the E_1' mode in the D_{5h} form and the total intensity of the coincident D_{5d} absorptions in this spectral region is 0.7. Hence, both the frequency splitting and the intensity ratios may be used as a probe to the conformation assumed by the molecules of ferrocene.

Besides the general excellent agreement between the observed spectrum of ferrocene in the argon matrix and the calculated spectrum for the D_{5h} conformation, it can also be seen in Figure 2 (see also Table 3) that the spectral profile in the 450-530 cm^{-1} conformation sensitive region clearly demonstrates that the ferrocene molecules exist in the matrix in the D_{5h} conformation: the $E_1'-A_2''$ band splitting ($\Delta\nu = 19 \text{ cm}^{-1}$) is as predicted for this conformation, and the $I^{\text{IR}}(E_1')/I^{\text{IR}}(A_2'')$ intensity ratio (2.1) is also close to the expected value, though slightly lower than this latter. Note that in spite of the possible less good theoretical prediction of the $I^{\text{IR}}(E_1')/I^{\text{IR}}(A_2'')$ ratio by the present calculations (for example, the B3LYP/m6-31G(d) calculations reported in [29] yield this intensity ratio as equal to 2.5, closer to the present experimental value for the compound in argon matrix), as it will be discussed in detail later on the $I^{\text{IR}}(E_1')/I^{\text{IR}}(A_2'')$ intensity ratio seems indeed to be rather sensitive to the environment, reducing its value with the polarity of the media.

Another observation to note here is that all bands in the experimental spectrum of matrix isolated ferrocene exhibit splitting due to trapping of molecules in different matrix sites. This is a well known phenomenon [46] that has been found to be particularly notable for ring-containing compounds isolated in solid argon [47,48]. The fact that both E_1' and A_2'' bands appear split allows a doubtless assignment of the splitting to the trapping of molecules in different matrix sites and not to the breakdown of the D_{5h} symmetry.

Once the experimental confirmation of the characteristic infrared signature of the minimum energy D_{5h} form of ferrocene was achieved and the existence of this form in the gas phase confirmed through the matrix-isolation studies above described, the experimental investigation of the neat compound in solid phase was initiated.

The first step was to perform temperature variation infrared studies for the compound diluted in a KBr pellet. The starting material was first confirmed to correspond to the monoclinic polymorph of ferrocene by obtaining its X-ray powder diffraction pattern (see Figure S1 in Supporting Information) and DSC traces from room temperature to above the melting point ($T_{\text{fus}} = 447.8 \pm 0.2 \text{ K}$, $\Delta_{\text{fus}}H = 18.3 \pm 0.2 \text{ kJ mol}^{-1}$, see Figure S2; literature values: $T_{\text{fus}} = 447.2 \text{ K}$, $\Delta_{\text{fus}}H = 18.3 \text{ kJ mol}^{-1}$ [49]). The room temperature spectrum of the monoclinic variety of the compound is presented in Figure S3 and the corresponding band assignments presented in Table 4. The sample was then cooled and spectra collected at different temperatures down till 20 K. Two cooling/re-warming cycles were performed. At the monoclinic-triclinic λ -transition ($\sim 169 \text{ K}$) fully reversible noticeable spectral changes could be

observed, in agreement with the phase change. The changes, though being subtle, can be noticed in the whole spectra (see Table 4 for assignments), but they are particularly evident in the 450-530 cm^{-1} and 750-870 cm^{-1} (νCH) regions, as shown in Figure 4. The data obtained in these experiments provided the characteristic infrared signature of the triclinic polymorph. It shall be noticed that below the λ -transition temperature the spectrum did not change, indicating that for the compound in a KBr pellet the low temperature stable orthorhombic polymorph [41-44] could not be formed, despite the long time the sample was kept at low temperature and the two cooling/re-warming cycles performed.

The next experiment carried out in the present investigation was made as follows: ferrocene was sublimated using the same procedure used to prepare the argon matrices, but it was deposited alone on the cryostat cooled infrared transparent substrate (20 K). The result was the production of a thin film of amorphous solid ferrocene. The infrared spectrum of this sample is shown in Figure S4 (see also Table 4), their most relevant 450-530 cm^{-1} and 760-870 cm^{-1} spectral regions being also presented in Figure 4. The deposited sample was then heated to 200 K, re-cooled to 20 K and further re-warmed till room temperature.

Upon increasing the temperature of the deposited ferrocene amorphous solid sample, spectral changes started to be noticeable at about 90 K, and occur continuously until 200 K, with different patterns of variation between 90 and *ca.* 150 K and from this temperature up. Subsequent cooling of the sample till 20 K led to observation of a distinctive spectrum, with narrower bands characteristic of an ordered crystalline phase, which has to correspond to the low temperature stable orthorhombic polymorph of the compound. Figure S5 shows the infrared spectrum of this polymorph. As expected, re-heating of the sample till room temperature yield the characteristic spectral signature of the high-temperature stable monoclinic polymorph, in a process which starts at *ca.* 240 K [43].

The comparison of the spectra obtained in the two experiments above described, especially in the 450-530 cm^{-1} and 760-870 cm^{-1} spectral regions (see Figure 4), led to the following conclusions:

(i) The changes observed in the spectra obtained during the heating of the amorphous solid can be ascribed to an initial partial crystallization of the sample in the orthorhombic polymorph, at temperatures below 150 K, followed by crystallization of the remaining amorphous material in the triclinic modification at higher temperatures. The spectrum obtained at 150 K is in fact a superposition of those of the amorphous material and the characteristic spectrum of the orthorhombic polymorph obtained after re-cooling of the sample (see Figure 4), while that obtained at 200 K is a mixture of these two spectra plus that of the triclinic polymorph. Very interestingly, though at the λ -transition temperature (~ 169 K) the transition from the triclinic to the monoclinic polymorph could be expected to take place, the spectrum obtained at 200 K indicates that the major species present in the sample at that temperature are the triclinic and the

orthorhombic polymorphs, though the presence of the monoclinic polymorph cannot be excluded due to the similarity of the spectra of the triclinic and monoclinic polymorphs. It is possible that in the presence of the stable orthorhombic modification the λ -transition between the two metastable polymorphs is diffculted. It is also interesting to note that, in a similar way to our observations, crystallization of ferrocene from alcoholic solutions into the orthorhombic polymorph has been reported only at temperatures below 110 K, the triclinic polymorph appearing as the dominant polymorph formed during crystallization of the compound from these solutions at temperatures below the λ -transition temperature (above this temperature the monoclinic modification is formed) [42].

(ii) The orthorhombic polymorph of ferrocene has the molecules of the compound in the eclipsed D_{5h} conformation [42]. We can also expect that in the amorphous state produced from the vapor, like observed in the cryogenic argon matrix, the molecules of ferrocene adopt the D_{5h} conformation. The broader profiles of the bands of the IR spectrum of the amorphous phase, compared to those of the orthorhombic crystal at the same temperature (20 K; see Figures 5-7), result from the more disordered structure of the glass, and not from a higher conformational disorder of the individual molecules. Accordingly, the $E_1'-A_2''$ band splitting observed in the 450-500 cm^{-1} spectral region for both phases is 19 cm^{-1} (*i.e.*, the same as observed for the D_{5h} isolated molecule in an argon matrix), and the $I^{\text{IR}}(E_1')/I^{\text{IR}}(A_2'')$ intensity ratio is also nearly the same in the two phases (1.6 in the amorphous and 1.5 in the orthorhombic crystal; note that the intensity ratios are different in the two spectra if we look to peak intensities instead, as properly, to the areas below the bands, due to the different band profiles). The $I^{\text{IR}}(E_1')/I^{\text{IR}}(A_2'')$ ratio for the amorphous and orthorhombic phases is, however, somewhat smaller than observed in case of the spectrum of the matrix isolated compound (2.1). Since in all cases the molecules are in the D_{5h} conformation, this difference in the $I^{\text{IR}}(E_1')/I^{\text{IR}}(A_2'')$ intensity ratio shall be attributed to the influence of the environment, with more polar media implying a smaller intensity ratio.

(iii) Contrarily to what happens for the orthorhombic phase, both the $E_1'-A_2''$ band splitting and the $I^{\text{IR}}(E_1')/I^{\text{IR}}(A_2'')$ intensity ratio are different in the spectra of the monoclinic and triclinic polymorphs, compared to that of the amorphous phase: 12 cm^{-1} and 0.8, and 14 cm^{-1} and 1.1, for monoclinic and triclinic phases, respectively. These differences shall be due predominantly to conformational effects. In the triclinic crystal, the molecules were found to adopt an equilibrium conformation where the two rings are rotated by 9 degrees from the eclipsed D_{5h} structure [40]. Though as mentioned before the structure of the individual molecules in the monoclinic crystal is not known, one can expect that the average angle between the two rings is at least slightly larger than in the triclinic polymorph. Under this assumption, we performed a simple simulation of the spectra of the three polymorphs in the conformationally sensitive 450-530 cm^{-1} range, where the spectra were built as average spectra of the B3LYP/LANL2DZ + cc-pVDZ calculated spectra for different values of the angle between the two cyclopentadienyl rings of ferrocene. In

the simulations, all calculated frequencies in this spectral region were scaled by 1.083 (the same factor as in the simulation of the spectra obtained in the matrix) and the intensities scaled so that the $I^{\text{IR}}(E_1')/I^{\text{IR}}(A_2'')$ intensity ratio for the D_{5h} structure equals that observed in the spectrum of the orthorhombic polymorph. Individual calculated component spectra were simulated by Lorentzian functions with full-width-at-half-band-maximum (FWHM) of 10 and 5 cm^{-1} for the E_1' and A_2'' bands, respectively, as observed in the orthorhombic crystal experimental spectrum. For simulation of the orthorhombic crystal spectrum, calculated spectra for structures with the ring torsion angle in the range 0-6 degrees (increment of 1 degree) were added. Since within this ring torsion angle interval the spectra of the various structures are virtually the same, the obtained spectrum is identical to that of the D_{5h} conformation. For the triclinic crystal spectrum simulation, spectra corresponding to structures with ring torsion angles between 0 and 18 degrees (center at 9 degrees, the experimental equilibrium value in this polymorph [40]) were used. Finally, for the simulation of the monoclinic crystal spectrum, structures with the ring torsion angle in the 0 to 28 degrees range (center: 14 degrees) were considered. The range of structures to simulate the monoclinic polymorph spectrum was chosen to attain the best possible fit between the simulated and experimental spectra within the simple adopted model. Though being very approximate (to improve the model, an estimation of the ring torsional potentials for the different polymorphs is required), the simulations qualitatively fit well the observations (Figure 5). Noteworthy, the calculated $I^{\text{IR}}(E_1')/I^{\text{IR}}(A_2'')$ intensity ratios for the orthorhombic, triclinic and monoclinic simulated spectra are 1.5, 1.2 and 0.9, in good agreement with the experimental values (1.5, 1.1 and 0.8, respectively).

In summary, the infrared experimental data obtained in this study for solid ferrocene demonstrate the relevance of the intermolecular interactions in determining the preferred conformations assumed by the individual molecules of the compound. As for the isolated molecule in a cryogenic argon matrix, the low temperature stable orthorhombic crystal exhibits a ordered structure with ferrocene molecules with an equilibrium eclipsed D_{5h} conformation and, at 20 K, with relatively small vibrational amplitudes associated with the ring torsional vibration (most probably within 6 degrees from the eclipsed conformation). In the triclinic polymorph, the equilibrium value for the ring torsion mode changes to 9 degrees, the vibrational amplitudes along this coordinate being significantly larger than for the orthorhombic polymorph (a value of about 10 degrees can be tentatively proposed, according to the simulations of the spectrum obtained at 160 K). Finally, in the monoclinic polymorph, we can tentatively propose, based on the simulations, an even larger equilibrium ring torsion angle (~ 15 degrees) for individual molecules in the crystal at room temperature, and corresponding vibrational amplitudes of *ca.* 15 degrees at room temperature. It seems also that the dynamic conformational disorder is not the only type of disorder playing a role in the monoclinic polymorph of ferrocene. Static disorder seems to play a role in this case as well, being the main

driving force for the triggering of the λ -transition between the essentially ordered at long-range-scale triclinic polymorph and the monoclinic form. Such disorder might, however, ultimately be also determined by the conformational dynamics and the gradual increase with temperature of the amplitude of the vibration along the ring torsional coordinate, in agreement with the proposition of Seiler and Dunitz [38].

3.2.2. 1-Bromoferrocene. Compared to unsubstituted ferrocene, the information available on 1-bromoferrocene is very scarce. However, its gas phase structure has been determined by microwave spectroscopy [30] and the 3D structure of its crystalline phase at room temperature determined by X-ray diffraction [51]. In agreement with our theoretical predictions, the gas phase microwave experiments showed that the eclipsed conformation of the two rings corresponds to the equilibrium geometry of the molecule of 1-bromoferrocene in the gas phase [30]. A similar arrangement has also been reported for other mono-substituted ferrocenes in gas phase, *e.g.*, 1-methylferrocene and 1-chloroferrocene [52,53]. Figure 6 shows the infrared spectrum (3200-450 cm^{-1} region) of the compound isolated in an argon matrix, and compares this spectrum with the B3LYP/LANL2DZ + cc-pVDZ calculated one. The assignments are presented in Table 5 (see Table S2 in the Supporting Information for full calculated spectra for both eclipsed and staggered conformations of the compound).

As in the case of ferrocene, the B3LYP/LANL2DZ + cc-pVDZ calculated spectrum fits nicely the experimental one, doubtless testifying the presence in the matrix of the eclipsed form of 1-bromoferrocene. Moreover, also for this molecule the experimental spectrum exhibits the usual matrix-site splitting.

It is also interesting to comment on the data obtained for the conformationally sensitive 450-530 cm^{-1} spectral region. According to the calculations, in this region both eclipsed and staggered conformations have two close bands at higher frequencies and a single band at lower frequency. The higher frequency bands were predicted at 504 and 502 cm^{-1} in the eclipsed form and at 486 and 483 cm^{-1} in the staggered, while the lower frequency band is predicted at 485 and 472 cm^{-1} in the eclipsed and staggered forms, respectively (see Tables 5 and S2). The calculated band splitting from the average position of the two higher frequency bands to the lower frequency band thus amount to 18 cm^{-1} in the eclipsed conformation and to 12 cm^{-1} in the staggered form. The experimental average frequencies for the components of the absorptions corresponding to the two higher and the lower frequency bands are 504 and 488 cm^{-1} , *i.e.*, $\Delta\nu = 16 \text{ cm}^{-1}$, closer to the predicted value for the eclipsed conformation. In turn, as it could be expected, the observed $I^{\text{IR}}(\text{higher frequency bands})/I^{\text{IR}}(\text{lower frequency band})$ intensity ratio (1.8) is also closer to the predicted value for the eclipsed form (2.0) than for the staggered one (0.8) (the calculated values for the intensity ratio are corrected values obtained by using the scale factor transferred from ferrocene and that result from the fitting of the $I^{\text{IR}}(E_1')/I^{\text{IR}}(A_2')$

calculated intensity ratio for that molecule to the corresponding observed ratio in the argon matrix spectrum; as discussed above, this scaling accounts for the partial environment dependence of the considered band intensity ratio).

Contrarily to ferrocene, only one polymorph of 1-bromoferrocene is known. Very interestingly, in the crystal ($P2_1/c$, $Z = 8$; monoclinic) the molecules of 1-bromoferrocene exist in both the eclipsed and staggered conformation [51]. In the crystal structure, four molecules form tetramers *via* intermolecular C–H \cdots Br hydrogen bonds between the C–H groups of molecules with eclipsed conformation and the Br atom of molecules with staggered conformation, and also C–H \cdots Br hydrogen bonds between molecules with eclipsed conformations (see Figure S6 in the Supporting Information). The tetramers are linked to each other by weak C–H $\cdots\pi$ interactions along the a axis of the crystal [51].

The infrared spectrum of the crystal (room temperature, in a KBr pellet) is shown in Figure 7 (assignments are provided in Table 6). The sample was checked by obtaining its DSC traces from room temperature to above the melting point ($T_{\text{fus}} = 306.4 \pm 0.1$ K, $\Delta_{\text{fus}}H = 14.2 \pm 0.4$ kJ mol $^{-1}$, see Figure S7 in the Supporting Information; literature: $T_{\text{fus}} = 304\text{--}305$ K [54], enthalpy of fusion not previously reported). Figure 7 shows also a simulated spectrum obtained based on the performed B3LYP/LANL2DZ + cc-pVDZ calculations for the eclipsed and staggered conformations. The spectrum was built by adding the calculated spectra of the two conformations, broadened by Lorentzian functions centered at the scaled frequencies and with FWHM = 10 cm $^{-1}$. As it can be seen in this Figure, the simulated spectrum generally reproduces well the observed spectrum, in spite of being based in calculations performed on the isolated molecules. This can be taken as an indication that the intermolecular interactions operating in the crystal do not perturb considerably the intramolecular vibrational modes. It can then be concluded that intermolecular interactions are rather weak, a conclusion that is also supported by the low melting point and enthalpy of fusion of the compound, nevertheless enough relevant to affect the potential energy profile of the molecule along its softest internal coordinate, which determines the relative orientation of the two rings. In fact, it is particularly fascinating that in the crystal of 1-bromoferrocene molecules adopt, besides the eclipsed conformation, the staggered conformation, which as doubtlessly proved by both the above described theoretical and matrix isolation infrared studies (as well as previously reported microwave spectroscopy results [30]) corresponds to the transition state geometry along the ring torsional coordinate for the isolated molecule of the compound. This is, then, a notable example of intermolecularly-induced perturbation of the conformational order existing in the isolated molecule, while the intermolecular interactions select not just a conformation that does not correspond to a minimum on the potential energy surface of the isolated molecule, but specifically selects that corresponding to a transition state. As it will be shown in the next

section, an even more remarkable example of such type of interplay between intra- and intermolecular forces occurs for 1,1'-dibromoferrocene.

3.2.3. **1,1'-Dibromoferrocene.** In spite of the well-recognized practical relevance of 1,1'-dibromoferrocene in the synthesis of ferrocene derivatives [55], there are no many structural studies on this compound. To the best of our knowledge, no theoretical calculations had been performed on this molecule hitherto, or its gas phase structure determined; the available vibrational data concern only the infrared and Raman spectra of the compound as a liquid film [56]. However, a crystal structure of 1,1'-dibromoferrocene has been reported (at 100 K) [57].

According to the theoretical calculations performed on the isolated molecule of 1,1'-dibromoferrocene in the present study (see Section 3.1), in the gas phase the molecule exists in two different two-fold minima of C_2 symmetry, with eclipsed rings and Br atoms opposed to H atoms (C_2 -I and C_2 -II; see Figure 1). The C_2 -I conformer is predicted by the calculations as more stable than C_2 -II by 0.82 kJ mol^{-1} ($\Delta G_{298} = 1.25 \text{ kJ mol}^{-1}$; equilibrium room temperature populations: C_2 -I, 62%; C_2 -II, 38%). Figure 8 shows the infrared spectrum (3200-450 cm^{-1} region) of the compound isolated in an argon matrix. This spectrum is well reproduced by the theoretical spectrum shown in the same Figure, which was constructed by adding the B3LYP/LANL2DZ + cc-pVDZ calculated infrared spectra of conformers C_2 -I and C_2 -II weighted by their theoretically estimated relative populations in gas phase prior to deposition. The assignments are given in Table 7, while the calculated spectra of all relevant conformations of 1,1'-dibromoferrocene are presented in Table S2 (Supporting information). The good agreement between the experimental and theoretical spectra confirms the composition of the room temperature gas phase equilibrium and, in particular, the greater stability of conformer C_2 -I in this phase.

Since the theoretical calculations predict a lower energy barrier for interconversion between the two conformers, the possibility of thermally changing the relative populations of the two conformers by increasing the temperature of the matrix was attempted. The results are shown in Figure 9. It is clear from this Figure that the increase of the temperature of the matrix from 15 to 35 K led to conversion of conformer C_2 -I into C_2 -II. This result implies that the relative order of stability of the conformers in the matrix is the opposite of that existing in the gas phase, with the C_2 -II form being more stable than C_2 -I. Indeed, upon increasing the matrix temperature the populations of the two conformers trapped from the room temperature vapor of the compound, and kept in the low temperature matrix as a metastable system, tend to adjust to the equilibrium of the low temperature [46]. This implies that the higher energy conformer in the matrix media must convert into the lower energy form (and never the opposite). The

stabilization of the C₂-II form in relation to C₂-I in the matrix (compared to gas phase) can be explained taking into account the larger dipole moment of C₂-II (2.28 D; vs. 0.35 D of C₂-I).

In the studies performed on the neat solid 1,1'-dibromoferrocene, we began with the characterization of the starting material, by obtaining its X-ray powder diffraction pattern (Figure S8, Supporting Information), which was found to fit well the theoretically predicted one for the previously reported X-ray crystal structure of the compound [57]. On the other hand, the DSC study of the sample allowed for the characterization of the original material and revealed the existence of a new polymorph (polymorph II), which was obtained after melting of the original polymorph and subsequent cooling the sample down to a temperature slightly below the room temperature.

Figure 10(Ia) shows a typical DSC curve obtained on heating the original compound (polymorph I) from room temperature to 333 K, at a scanning rate of 10 K min⁻¹. Only one endothermic transition was observed, at the expected temperature of fusion of this polymorph ($T_{\text{fus}} = 325.4 \pm 0.1$ K; $\Delta_{\text{fus}}H = 22.9 \pm 0.7$ kJ mol⁻¹; literature: $T_{\text{fus}} = 327\text{-}328$ K [56], enthalpy of fusion not previously reported). The nature of this transition was further confirmed by polarized light optical microscopy (PLTM) experiments (Figure 11(a)).

Cooling molten 1,1'-dibromoferrocene was carried out at 5 K min⁻¹. Examples of DSC crystallization curves are given in Figure 10(II). The DSC traces recorded in heating scans following these cooling experiments are shown in Figure 10(Ib2-f2). From the obtained thermograms, it is evident that crystallization of molten 1,1'-dibromoferrocene often gives rise to mixtures of polymorphs I and II in variable amounts. Polymorph II melts at $T_{\text{fus}} = 320.2 \pm 0.1$ K, *i.e.*, it has a melting point ~5 degrees below that of polymorph I. A single value for the enthalpy of fusion could be achieved for this polymorph ($\Delta_{\text{fus}}H \approx 22$ kJ mol⁻¹), as in all other experiments a visible mixture of both forms was obtained. In these cases, the sum of form I and form II fusion enthalpies are similar to the fusion enthalpy of form I, which confirms that the melt fully crystallized in the cooling runs.

The thermal behavior of 1,1'-dibromoferrocene was also studied by DSC in other experimental conditions such as cooling rates ranging from 10 to 2 K min⁻¹, annealing at temperatures of 283 and 288 K. It is worth noting that a particular behavior observed in the cooling runs could not be ascribed to a specific behavior in the subsequent heating run.

The existence of the second polymorph of 1,1-dibromoferrocene has been subsequently confirmed by temperature variation X-ray powder diffraction (see Figure S8), which also allowed also to conclude that polymorph I corresponds to the stable form of the compound at 283 K, as well as by PLTM, where observation of both polymorphs melting processes could be achieved (Figure 11). PLTM cooling/heating experiments were carried out on a small amount of compound dispersed as separated particles in a glass pan. In these conditions liquid

crystallization was observed between 295 and 265 K, Figure 11(b). The heating curves of these samples undoubtedly reveal the presence of both polymorphs, Figure 11(c).

Very unfortunately, it was not possible to isolate a single crystal of polymorph II to undertake its 3D structure determination by X-ray. Nevertheless some relevant information on the new polymorph could be obtained by infrared spectroscopy. A sample of the compound (polymorph I) was diluted in a KBr pellet and its infrared spectra obtained as a function of temperature. The room temperature spectrum is shown in Figure 12 (assignments are given in Table 8). Decreasing of the temperature of the sample down to 20 K did not lead to any noticeable spectral change, except the usual band narrowing, which in this case was indeed found to be quite modest. On the other hand, changes in the infrared spectrum were quite pronounced at the melting of the sample (Figure 13). As it could be expected, cooling/heating experiments mimicking those performed in the DSC experiments described above, allowed to generate polymorph II, leading to observation of the first characteristic spectral changes due to sample melting at a temperature about 5 K below that of the original sample. Though we were not able to produce, under these experimental conditions, a pure crystalline sample of polymorph II (both decreasing the temperature below 288 K or annealing the sample at this or higher temperature led to preferential crystallization of polymorph I, while decreasing the temperature only to above 288 K without waiting before re-warming led to incomplete crystallization and contamination of the spectrum of polymorph II with that of the melt), it was observed that the IR spectra of the two polymorphs are undistinguishable in practice. Such observation allows to conclude that the individual molecules in the crystals of the two polymorphs shall exist in the same conformation and that the intermolecular packing forces in the crystals are not strong enough to perturb considerably the intramolecular vibrational modes. Nevertheless, and this is the most intriguing observation we made on this fascinating molecule, the intermolecular forces in the crystals of 1,1'-dibromoferrocene are still sufficiently strong to affect the potential energy profile of the molecule along its softest internal coordinate, which determines the relative orientation of the two rings, selecting as preferred conformation in the crystals not just a conformation different from the minimum energy structures in the gas phase (C_2 -I and C_2 -II, also observed to be present in the studied cryogenic argon matrix), but the one that corresponds to the *highest* energy transition state along this coordinate (the C_{2v} eclipsed structure, with the two bromine atoms opposed to each other; see Figure 1, and also Figure S9, where the X-ray 3D structure of polymorph I of the compound is drawn according to the data obtained in ref [57]).

It is interesting to note that the surprising structure adopted by the molecules of 1,1'-dibromoferrocene in the crystalline state was recognized in the original X-ray study [57], where the authors explicitly attributed the observed arrangement to crystal packing effects (the fact that the C_{2v} structure is that having the largest dipole moment, 2.82 D, among all possible

structures differing in the relative orientation of the two rings in the molecule may play a role on this). In fact, in the other few 1,1'-dibromoferrocenes already studied (bearing additional substituents at the rings) the molecules were found to exist in eclipsed conformations but where (like in the C₂-I and C₂-II minimum energy conformations for 1,1'-dibromoferrocene) the bromine atoms oppose to H atoms and not to each other [58,59].

3.3. Conclusions

The interplay between intermolecular interactions in the crystalline state and the intramolecular conformational potential energy landscapes for cyclopentadienyl rings in ferrocene, 1-bromoferrocene and 1,1'-dibromoferrocene was investigated. It was shown that intermolecular interactions induce conformational disorder, leading to presence in several polymorphic forms of the compounds of monomeric units with conformations far from those corresponding to minimum energy structures in the gas phase and found also to be present for monomers of the compounds isolated in cryogenic matrices. The results presented in this article thus represent enlightening examples of intermolecularly-induced conformational disorder in solid phase and of its relevance to polymorphism.

In both ferrocene and 1-bromoferrocene, staggered (or nearly staggered) conformations, which correspond to transition state structures in the gas phase, were found to be present in the room temperature polymorphs. On the other hand, 1,1'-Dibromoferrocene, which exists in both gas phase and low temperature argon matrix in two conformers (C₂-I and C₂-II), with eclipsed cyclopentadienyl moieties and Br atoms opposed to H atoms, was shown to have its molecules in the crystalline phases (both polymorph I and II) in a conformation corresponding not just to a different conformation, but to the *highest* energy transition state along the ring torsional coordinate (the C_{2v} eclipsed structure, with the two bromine atoms opposed to each other).

On the whole, combined use of quantum chemistry, infrared spectroscopy, differential scanning calorimetry, polarized light thermomicroscopy and powder diffraction allowed the detailed structural and spectroscopic characterization of the three studied compounds in various experimental conditions, and to gather information about their most relevant thermodynamic properties, including identification of a new polymorph of 1,1'-dibromoferrocene.

Supporting Information: Tables S1 and S2, with optimized Cartesian coordinates and calculated IR spectra for minima and transition state structures of ferrocene, 1-bromoferrocene and 1,1'-dibromoferrocene; Figures S1 and S2, with X-ray powder diffractogram and DSC heating curve for the original sample of ferrocene used in this study; Figures S3, S4 and S5,

with observed IR spectra of the monoclinic polymorph (room temperature), amorphous phase (20 K) and orthorhombic polymorph (20 K) of ferrocene; Figures S6 and S7 with view of tetramer unit in the crystal of 1-bromoferrocene and DSC heating curve of the original sample of this compound used in the present study; Figure S8 and Figure S9, with the X-ray powder diffractograms obtained for 1,1'-dibromoferrocene and view of the tetramer unit in polymorph I of the compound.

Acknowledgements: The authors are grateful to Prof. Luís M. N. B. F. Santos (University of Porto, Portugal) for having provided the purified samples of the compounds studied in this work and Profs. José António Paixão and Manuela R. Silva (Department of Physics, University of Coimbra) for obtaining the X-ray powder diffraction patterns of the original samples. The research was supported by the Portuguese *Fundação para a Ciência e a Tecnologia* (FCT, Project PTDC/QUI/111879/2009). C.M.N. also acknowledges FCT by the post-doctoral grant ref. SRH/BPD/86021/2012.

References

- [1] A. Gómez-Zavaglia, I. D. Reva and R. Fausto, *Phys. Chem. Chem. Phys.*, **5** (2003) 41.
- [2] L. Khriachtchev, E. Maçôas, M. Pettersson and M. Räsänen, *J. Am. Chem. Soc.*, **124** (2002) 10994.
- [3] G. F. X. Schertler, *Nature*, **453** (2008) 292.
- [4] J. Saunders, *Nature Rev. Microbiol.*, **1** (2003) 6.
- [5] D. Sabbert, S. Engelbrecht and W. Junge, *Nature*, **381** (1996) 623.
- [6] A. Nangia, *Acc. Chem. Res.*, **41** (2008) 595.
- [7] H. G. Brittain, *Spectroscopy*, **15** (2000) 34.
- [8] J. Bernstein and A. T. Hagler, *J. Am. Chem. Soc.*, **100** (1978) 673.
- [9] J. Bernstein, *Polymorphism in Molecular Crystals*, Oxford University Press, ISBN 0 19 850605, 2002.
- [10] J. J. Gerber, M. R. Caira and A. P. Lötter, *J. Cryst. Spec. Res.*, **23** (1993) 863.
- [11] J. R. Smith, W. Xu and D. Raftery, *J. Phys. Chem. B*, **110** (2006) 7766.
- [12] J. Bauer, S. Spanton, R. Henry, J. Quick, W. Dziki, W. Porter and J. Morris, *Pharm. Res.*, **18** (2001) 859.
- [13] L. H. Thomas, G. A. Craig, M. J. Gutmann, A. Parkin, K. Shankland and C. C. Wilson, *CrystEngComm*, **13** (2011), 3349.
- [14] P. Negrier, M. Barrio, M. Zuriaga, S. C. Pérez, J. L. I. Tamarit and D. Mondieig, *MATEC Web of Conferences*, **3** (2013) 01064.
- [15] J. Bernstein, J. Davey and J.-O. Henk, *Angew. Chem. Int. Ed.*, **38** (1999) 3440.
- [16] T. M. R. Maria, R. A. E. Castro, S. S. Bebiano, M. Ramos Silva, A. Matos-Beja, J. Canotilho and M. E. S. Eusébio, *Cryst. Growth Des.*, **10** (2010) 1194.
- [17] R. Sabbah, A. X. Wu, J. S. Chickos, M. L. P. Leitão, M. V. Roux and L. A. Torres, *Thermochim. Acta*, **331** (1995) 93.
- [18] M. J. Frisch, G. W. Trucks, H. B. Schlegel, G. E. Scuseria, M. A. Robb, J. R. Cheeseman, J. A. Montgomery, Jr., T. Vreven, K. N. Kudin, J. C. Burant, J. M. Millam, S. S. Iyengar, J. Tomasi, V. Barone, B. Mennucci, M. Cossi, G. Scalmani, N. Rega, G. A. Petersson, H. Nakatsuji, M. Hada, M. Ehara, K. Toyota, R. Fukuda, J. Hasegawa, M. Ishida, T. Nakajima, Y. Honda, O. Kitao, H. Nakai, M. Klene, X. Li, J. E. Knox, H. P. Hratchian, J. B. Cross, V. Bakken, C. Adamo, J. Jaramillo, R. Gomperts, R. E. Stratmann, O. Yazyev, A. J. Austin, R. Cammi, C. Pomelli, J. W. Ochterski, P. Y. Ayala, K. Morokuma, G. A. Voth, P. Salvador, J. J. Dannenberg, V. G. Zakrzewski, S. Dapprich, A. D. Daniels, M. C. Strain, O. Farkas, D. K. Malick, A.D. Rabuck, K. Raghavachari, J.B. Foresman, J.V. Ortiz, Q. Cui, A.G. Baboul, S. Clifford, J. Cioslowski, B.B. Stefanov, G. Liu, A. Liashenko, P. Piskorz, I. Komaromi, R.L. Martin, D. J. Fox, T. Keith, M. A. Al-Laham, C. Y. Peng, A.

- Nanayakkara, M. Challacombe, P. M. W. Gill, B. Johnson, W. Chen, M. W. Wong, C. González and J. A. Pople, GAUSSIAN 03, Revision C.02. Gaussian, Inc., Wallingford CT, 2004.
- [19] A.D. Becke, *Phys. Rev. A*, **38** (1988) 3098.; C.T. Lee, W.T. Yang and R.G. Parr, *Phys. Rev. B*, **37** (1988) 785.
- [20] H. Dunning, *J. Chem. Phys.*, **90** (1989) 1007).
- [21] E. R. Davidson, *Chem. Phys. Lett.*, **260** (1996) 514.
- [22] P. J. Hay and W. R. Wadt, *J. Chem. Phys.*, **82** (1985) 299.
- [23] S. Corani, A. Haaland, T. Helgaker and P. Jørgensen, *ChemPhysChem*, **7** (2006) 245.
- [24] T. P. Grayaznova, S. A. Katsyuba, V. A. Milyukov and O. G. Sinyashin, *J. Organomet. Chem.*, **695** (2010) 2586.
- [25] Y. Yang, M. N. Weaver and K. M. Merz, Jr., *J. Phys. Chem. A*, **113** (2009) 9843.
- [26] G. A. Zhurko, Chemcraft (version 1.6), <http://www.chemcraftprog.com>.
- [27] R. K. Bohn and A. Haaland, *J. Organomet. Chem.*, **5** (1966) 470.
- [28] A. Haaland and J. E Nielsen, *Acta Chem. Scand.*, **22** (1968) 2653.
- [29] N. Mohammadi, A. Ganesan, C. T. Chantler and F. Wang, *J. Organomet. Chem.*, **713** (2012) 51.
- [30] B. J. Drouin, T. G Lavaty, P. Cassak and S. G. Kukolich, *J. Chem. Phys.*, **107** (1997) 6541.
- [31] E. O. Fischer and W. Pfab, *Z. Naturforsch. B*, **7** (1952) 377.
- [32] P. F. Eiland and R. Pepinsky, *J. Am. Chem. Soc.*, **74** (1952) 4971.
- [33] J. D. Dunitz and L. E. Orgel, *Nature (London)*, **171** (1953) 121.
- [34] J. D. Dunitz, L. E. Orgel and A Rich, *Acta Cryst.*, **9** (1956) 373.
- [35] J. W. Edwards, G. L. Kington and R. Mason, *Trans. Faraday Soc.*, **56** (1960) 660.
- [36] B. T. M. Willis, *Acta Cryst.*, **13** (1960) 1088.
- [37] A. J. Campbell, C. A. Fyfe, D. Harold-Smith and K. R. Jeffrey, *Mol. Cryst. Liq. Cryst.*, **36** (1976) 1.
- [38] P. Seiler and J. D. Dunitz, *Acta Cryst. B*, **35** (1979) 1068.
- [39] F. Takusagawa and T. F. Koetzle, *Acta Cryst. B*, **35** (1979) 1074.
- [40] P. Seiler and J. D. Dunitz, *Acta Cryst. B*, **35** (1979) 2020.
- [41] K. Ogasahara, M. Sorai and H. Suga, *Chem. Phys. Lett.*, **68** (1979) 457.
- [42] P. Seiler and J. D. Dunitz, *Acta Cryst. B*, **38** (1982) 1741.
- [43] J.-F. Bérrar, G. Calvarin, D. Weigel, K. Chhor and C. Pommier, *J. Chem. Phys.*, **73** (1980) 438.
- [44] S. Toscani, P. Oliveira and R. Céolin, *J. Solid State Chem.*, **164** (2002) 131.
- [45] N. Mohammadi, F. Wang, S. Best, D. Appadoo and C. T. Chantler, pre-print available at arXiv:1306.0633. <http://arxiv.org/pdf/1306.0633v1>

- [46] For details on the matrix isolation infrared spectroscopy technique see, for example: R. Fausto, Ed., "Low Temperature Molecular Spectroscopy", NATO-ASI Series C483, Kluwer Inc., Amsterdam (Holland), 1996; A. Barnes, W. J. Orville-Thomas, R. Gaufrhs and A. Muller, Eds., "Matrix Isolation Spectroscopy", Springer, 1981; I. R. Dunkin, "Matrix Isolation Techniques: A Practical Approach", Oxford University Press, 1998.
- [47] B. M. Giuliano, I. Reva, L. Lapinski and R. Fausto, *J. Chem. Phys.* **136** (2012) Art. N° 024505.
- [48] N. Kuş, S. Bayarı and R. Fausto, *J. Phys. Chem. B*, **117** (2013) 13543.
- [49] J. W. Edwards and G. I. Kington, *Trans. Faraday Soc.*, **58** (1962) 1334.
- [50] J. S. Bodenheimer and W. Low, *Spectrochim. Acta A*, **29** (1973) 1733.
- [51] A. S. Romanov, J. M. Mulroy, V. N. Khrustalev, M. Yu. Antipin and T. V. Timofeeva, *Acta Cryst. C*, **65** (2009) m426.
- [52] D. S. Margiolis, C. Tanjaron and S. G. Kukolich, *J. Chem. Phys.*, **117** (2002) 3741.
- [53] B. J. Drouin, J. J. Dannemiller and S. G. Kukolich, *J. Chem. Phys.*, **112** (2000) 747.
- [54] R. W. Fish and M. Rosenblum, *J. Org. Chem.*, **30** (1965) 1253.
- [55] I. R. Butler, *Inorg. Chem. Commun.*, **11** (2008) 15.
- [56] J. N. Willis, Jr., M. T. Ryan, F. L. Hedberg and H. Rosenberg, An Infrared and Raman Study of 1,1'-Disubstituted Ferrocene Compounds, Technical Report USA Air Force Materials Laboratory AFML-TR-67-238, Research and Technology Division, USA Air Force Systems Command, Wright-Patterson Air Force Base, Ohio, 1967 (approved for public release, 1972).
- [57] C. A. Hnetinka, A. D. Hunter, M. Zeller and M. J. G. Lesley, *Acta Cryst. E*, **60** (2004) m1806.
- [58] I. R. Butler, M. G. B. Drew, C. H. Greenwell, E. Lewis, M. Plath, S. Mussig and J. Szewczyk, *Inorg. Chem. Commun.*, **2** (1999) 576.
- [59] M. B. Hursthouse, S. J. Coles and I. R. Butler, Private Communication to the Cambridge Structural Database; reference No. CCDC 217925, refcode UJETEI. Cambridge Crystallographic Data Centre, 12 Union Road, Cambridge, England. 2003.

Captions to the figures

Figure 1. B3LYP/LANL2DZ + cc-pVDZ calculated ring torsion potential energy profiles for ferrocene (*top*), 1-bromoferrocene (*mid*) and 1,1'-dibromoferrocene (*bottom*). The vertical axes were drawn in the same scale to facilitate the comparison between the 3 curves. Positions of the zero-point vibrational levels ($\nu = 0$) for the shown minimum energy conformations are indicated.

Figure 2. Observed infrared spectrum of ferrocene isolated in an argon matrix, at 15 K (*top*), and simulated infrared spectrum for the minimum energy conformation of the compound (form D_{5h} ; *bottom*). The B3LYP/LANL2DZ + cc-pVDZ calculated frequencies, scaled by 0.984 (except for the ν_{CH} and Cp-Fe regions where scale factors of 0.957 and 1.083 were used, respectively), together with the calculated IR intensities, served to simulate the spectra shown in the figure by convoluting each peak with a Lorentzian function with a full width at half-maximum (FWHM) of 2 cm^{-1} . Note that the calculated intensities correspond to the area between the peaks, so that the intensities provided in Table 3 do not fit the peak intensities in the plot.

Figure 3. B3LYP/LANL2DZ + cc-pVDZ calculated frequencies (scaled) and infrared intensities for the bands in the conformational sensitive $530\text{-}450\text{ cm}^{-1}$ spectral range as a function of the relative orientation of the two cyclopentadienyl rings in ferrocene (indicated in degrees by the numbers in the figure, where 0° corresponds to the eclipsed D_{5h} conformation and 36° to the staggered D_{5d} structure).

Figure 4. Observed infrared spectra of neat solid ferrocene in the $450\text{-}530\text{ cm}^{-1}$ (*bottom*) and $760\text{-}870\text{ cm}^{-1}$ (*top*) spectral regions. The solid lines correspond to the orthorhombic (O), triclinic (T), monoclinic (M) and amorphous (A) phases; the dashed and dotted lines to spectra obtained during the heating of the amorphous phase at 150 and 200 K, respectively. The triclinic and monoclinic spectra were obtained at 160 K and room temperature, respectively, for the compound in KBr (the spectrum of the neat solid film at room temperature is virtually identical to that of that of the monoclinic polymorph in KBr). The amorphous and orthorhombic spectra were obtained for a film of the neat compound at 20 K, as described in the text.

Figure 5. $450\text{-}530\text{ cm}^{-1}$ spectral region of the infrared experimental (*top*) and simulated (*bottom*) spectra of the orthorhombic (O; dashed line), triclinic (T, solid line) and monoclinic (M, tick solid line). The experimental data is the same as shown in Figure 4. The simulated spectra were obtained by averaging of the B3LYP/LANL2DZ + cc-pVDZ calculated spectra for different values of the angle between the two cyclopentadienyl rings of ferrocene. All calculated frequencies were scaled by 1.083 and the intensities scaled so that the $I^{\text{IR}}(E_1')/I^{\text{IR}}(A_2'')$ intensity ratio for the D_{5h} structure is equal to that observed in the spectrum of the orthorhombic polymorph. Individual calculated component spectra were simulated by Lorentzian functions with FWHM of 10 and 5 cm^{-1} for the E_1' and A_2'' bands, respectively, as observed in the orthorhombic crystal experimental spectrum. For the orthorhombic crystal simulated spectrum, calculated spectra for structures with ring torsion angle in the range $0\text{-}6$ degrees (increment of 1 degree) were added; for the triclinic crystal spectrum simulation spectra corresponding to structures with ring torsion angles between 0 and 18 degrees (center: 9 degrees) were used; for the simulation of the monoclinic crystal spectrum structures with the ring torsion angle in the 0 to 28 degrees range (center: 14 degrees) were considered.

Figure 6. Observed infrared spectrum of 1-bromoferrocene isolated in an argon matrix, at 15 K (*top*), and simulated infrared spectrum for the minimum energy conformation of the compound (eclipsed form; *bottom*).

Figure 7. Observed room temperature infrared spectrum of crystalline 1-bromoferrocene in KBr pellet (*top*) and simulated infrared spectrum based on the sum of the B3LYP/LANL2DZ + cc-pVDZ calculated (scaled) spectra for the eclipsed and staggered conformations of the molecule of the compound (*bottom*). In the simulated spectrum bands were broadened by convoluting each peak with a Lorentzian function with a full width at half-maximum (FWHM) of 10 cm^{-1} . Note that the calculated intensities correspond to the area between the peaks, so that the intensities provided in Table 5 do not fit the peak intensities in the plot.

Figure 8. Observed infrared spectrum of 1,1'-dibromoferrocene isolated in an argon matrix, at 15 K (*top*), and simulated infrared spectrum constructed by adding the B3LYP/LANL2DZ + cc-pVDZ calculated infrared spectra of conformers C_2 -I and C_2 -II weighted by their theoretically estimated relative populations in gas phase prior to deposition (C_2 -I, 62%; C_2 -II, 38%) (*bottom*).

Figure 9. Observed infrared difference spectrum of 1,1'-bromoferrocene isolated in an argon matrix (spectrum obtained after warming of the matrix up to 35 K, minus spectrum of the as-deposited matrix at 15 K) (*top*), and simulated infrared difference spectrum obtained by subtracting the B3LYP/LANL2DZ + cc-pVDZ calculated spectrum of C_2 -I from that of C_2 -II.

Figure 10. DSC traces of 1,1'-dibromoferrocene samples: (I) obtained from two samples in heating runs, with heating rate of 10 K min^{-1} ; (a) original compound; (b2-f2) following melt crystallization at cooling rate -5 K min^{-1} ; (b2-e2) $m = 2.57\text{ mg}$; (f2) $m = 3.33\text{ mg}$; (II) obtained from melt cooling; (b1-e1) $m = 2.57\text{ mg}$; (f1) $m = 3.33\text{ mg}$.

Figure 11. PLTM images of 1,1'-dibromoferrocene samples. (a) original compound; heating rate 10 K min^{-1} ; magnification 200x; (b) melt cooling; cooling rate -5 K min^{-1} ; (c) heating run of the molten crystallized sample; heating rate 10 K min^{-1} ; magnification 50x.

Figure 12. Observed infrared spectrum of polymorph I of 1,1'-dibromoferrocene at room temperature.

Figure 13. Experimental infrared spectra of 1,1'-dibromoferrocene in the $1035\text{-}980\text{ cm}^{-1}$ range at different temperatures (*top*), and calculated spectra for the C_2 -I, C_2 -II and C_{2v} forms (*bottom*). According to the X-ray structure of polymorph I of the compound [57], in the room temperature crystal molecules assume the C_{2v} conformation. In the liquid phase, one can expect that the molecules assume the minimum energy conformations for the isolated molecule (C_2 -I and C_2 -II). Note also that the spectrum of the re-cooled melt at 293 K reveals that the compound had not yet fully crystallized at that temperature.

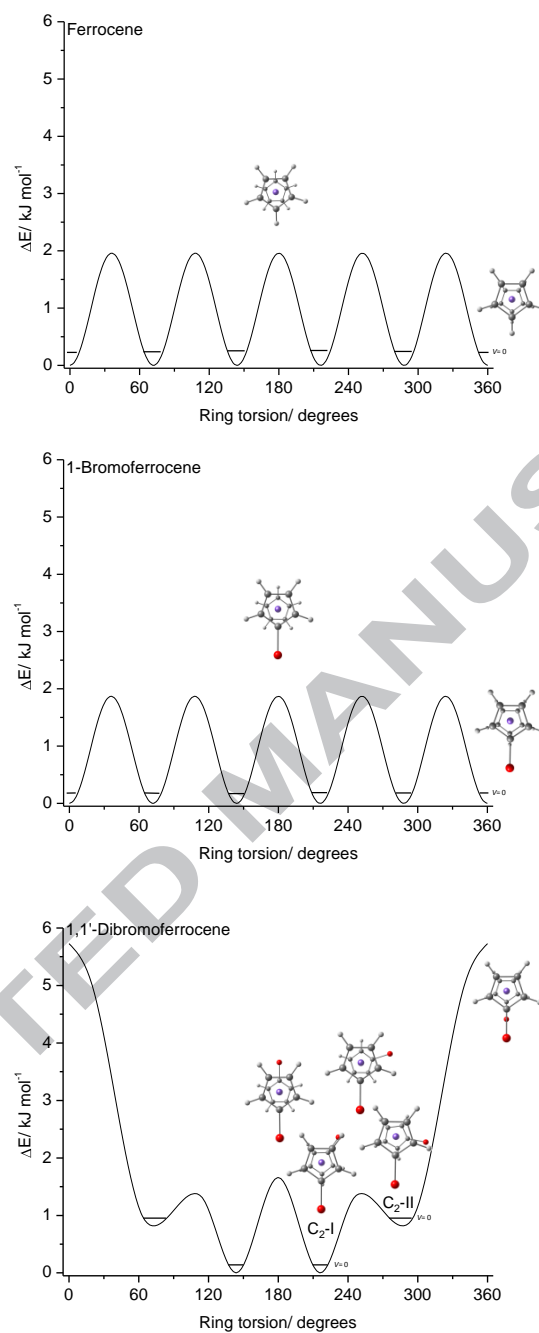


Figure 1. B3LYP/LANL2DZ + cc-pVDZ calculated ring torsion potential energy profiles for ferrocene (*top*), 1-bromoferrocene (*mid*) and 1,1'-dibromoferrocene (*bottom*). The vertical axes were drawn in the same scale to facilitate the comparison between the 3 curves. Positions of the zero-point vibrational levels ($\nu = 0$) for the shown minimum energy conformations are indicated.

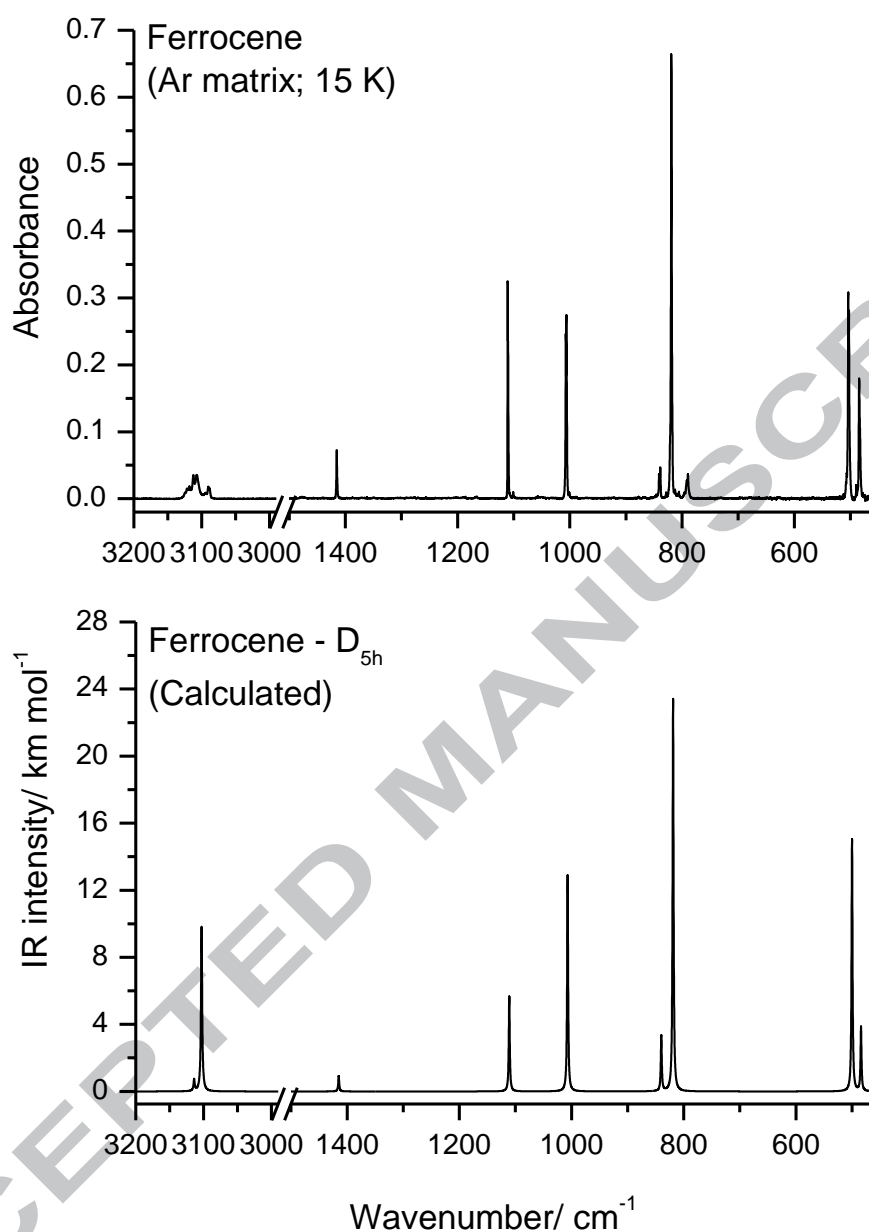


Figure 2. Observed infrared spectrum of ferrocene isolated in an argon matrix, at 15 K (*top*), and simulated infrared spectrum for the minimum energy conformation of the compound (form D_{5h}; *bottom*). The B3LYP/LANL2DZ + cc-pVDZ calculated frequencies, scaled by 0.984 (except for the ν CH and Cp-Fe regions where scale factors of 0.957 and 1.083 were used, respectively), together with the calculated IR intensities, served to simulate the spectrum shown in the figure by convoluting each peak with a Lorentzian function with a full width at half-maximum (FWHM) of 2 cm⁻¹. Note that the calculated intensities correspond to the area between the peaks, so that the intensities provided in Table 3 do not fit the peak intensities in the plot.

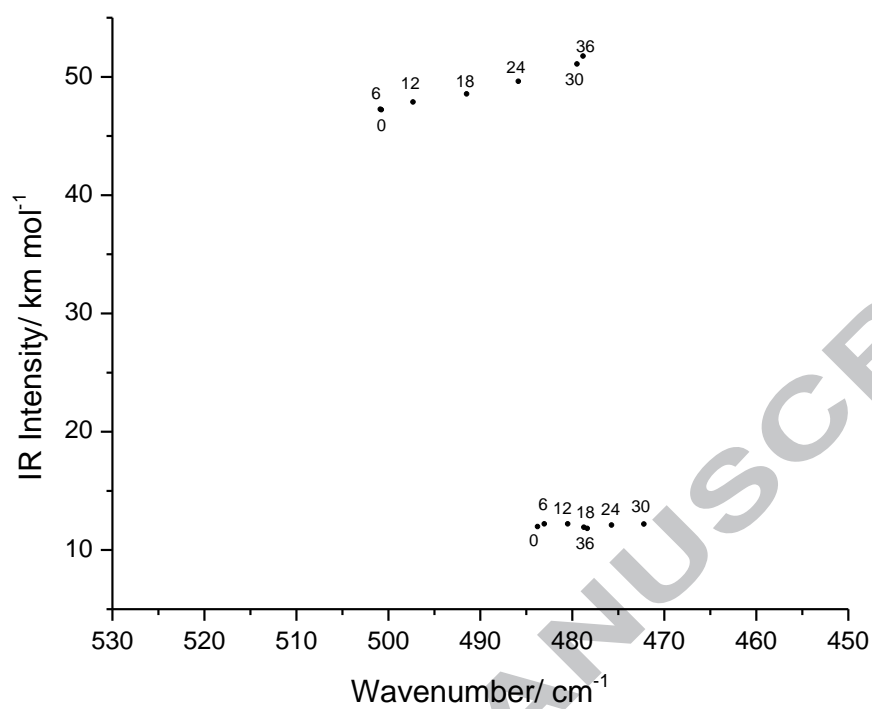


Figure 3. B3LYP/LANL2DZ + cc-pVDZ calculated frequencies (scaled) and infrared intensities for the bands in the conformational sensitive 530-450 cm^{-1} spectral range as a function of the relative orientation of the two cyclopentadienyl rings in ferrocene (indicated in degrees by the numbers in the figure, where 0° corresponds to the eclipsed D_{5h} conformation and 36° to the staggered D_{5d} structure).

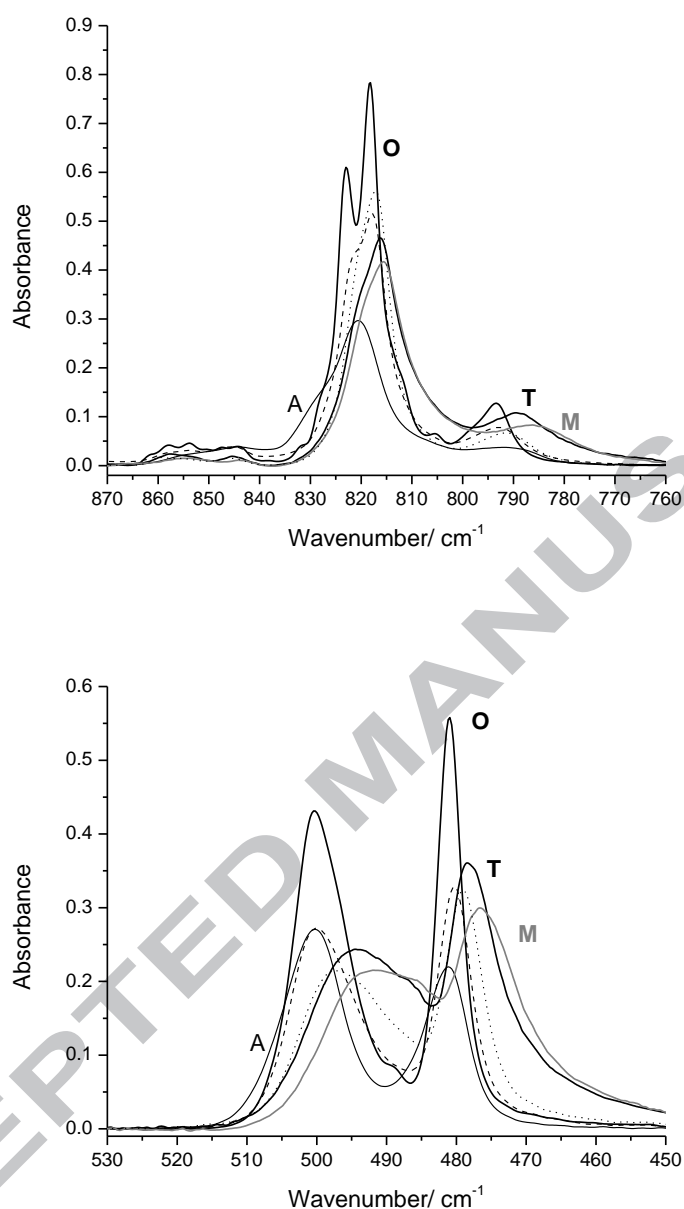


Figure 4. Observed infrared spectra of neat solid ferrocene in the 450-530 cm^{-1} (bottom) and 760-870 cm^{-1} (top) spectral regions. The solid lines correspond to the orthorhombic (O), triclinic (T), monoclinic (M) and amorphous (A) phases; the dashed and dotted lines to spectra obtained during the heating of the amorphous phase at 150 and 200 K, respectively. The triclinic and monoclinic spectra were obtained at 160 K and room temperature, respectively, for the compound in KBr (the spectrum of the neat solid film at room temperature is virtually identical to that of that of the monoclinic polymorph in KBr). The amorphous and orthorhombic spectra were obtained for a film of the neat compound at 20 K, as described in the text.

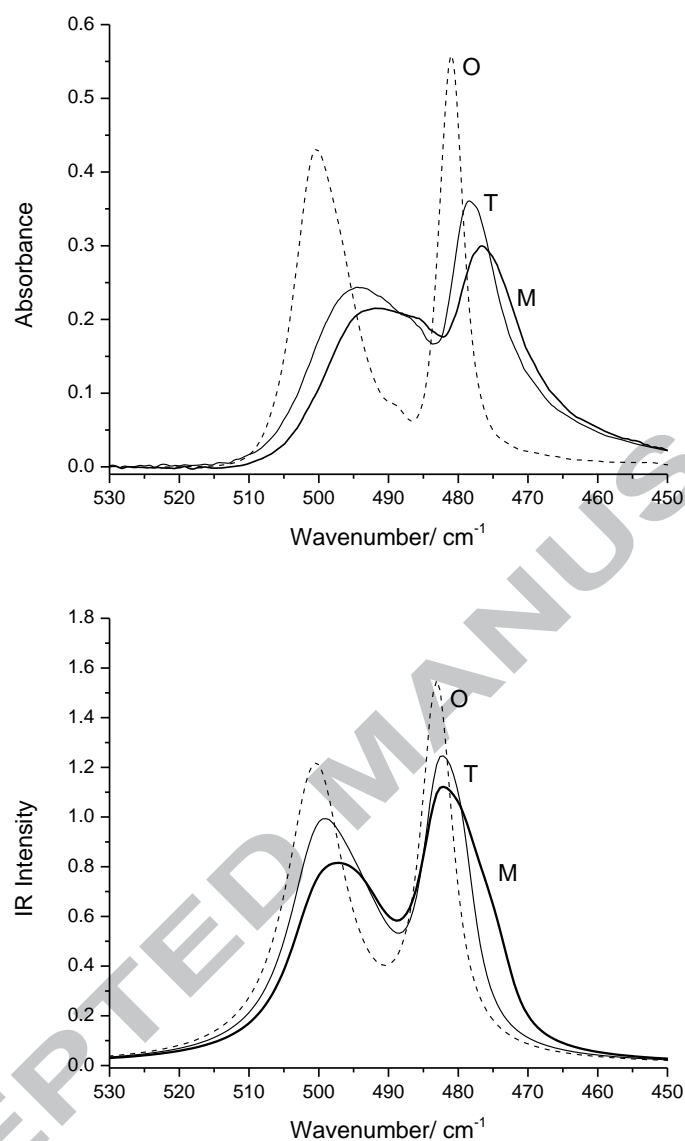


Figure 5. 450-530 cm^{-1} spectral region of the infrared experimental (*top*) and simulated (*bottom*) spectra of the orthorhombic (O; dashed line), triclinic (T, solid line) and monoclinic (M, tick solid line). The experimental data is the same as shown in Figure 4. The simulated spectra were obtained by averaging of the B3LYP/LANL2DZ + cc-pVDZ calculated spectra for different values of the angle between the two cyclopentadienyl rings of ferrocene. All calculated frequencies were scaled by 1.083 and the intensities scaled so that the $I^{\text{IR}}(E_1')/I^{\text{IR}}(A_2'')$ intensity ratio for the D_{5h} structure is equal to that observed in the spectrum of the orthorhombic polymorph. Individual calculated component spectra were simulated by Lorentzian functions with FWHM of 10 and 5 cm^{-1} for the E_1' and A_2'' bands, respectively, as observed in the orthorhombic crystal experimental spectrum. For the orthorhombic crystal simulated spectrum, calculated spectra for structures with ring torsion angle in the range 0-6 degrees (increment of 1 degree) were added; for the triclinic crystal spectrum simulation spectra corresponding to structures with ring torsion angles between 0 and 18 degrees (center: 9 degrees) were used; for the simulation of the monoclinic crystal spectrum structures with the ring torsion angle in the 0 to 28 degrees range (center: 14 degrees) were considered.

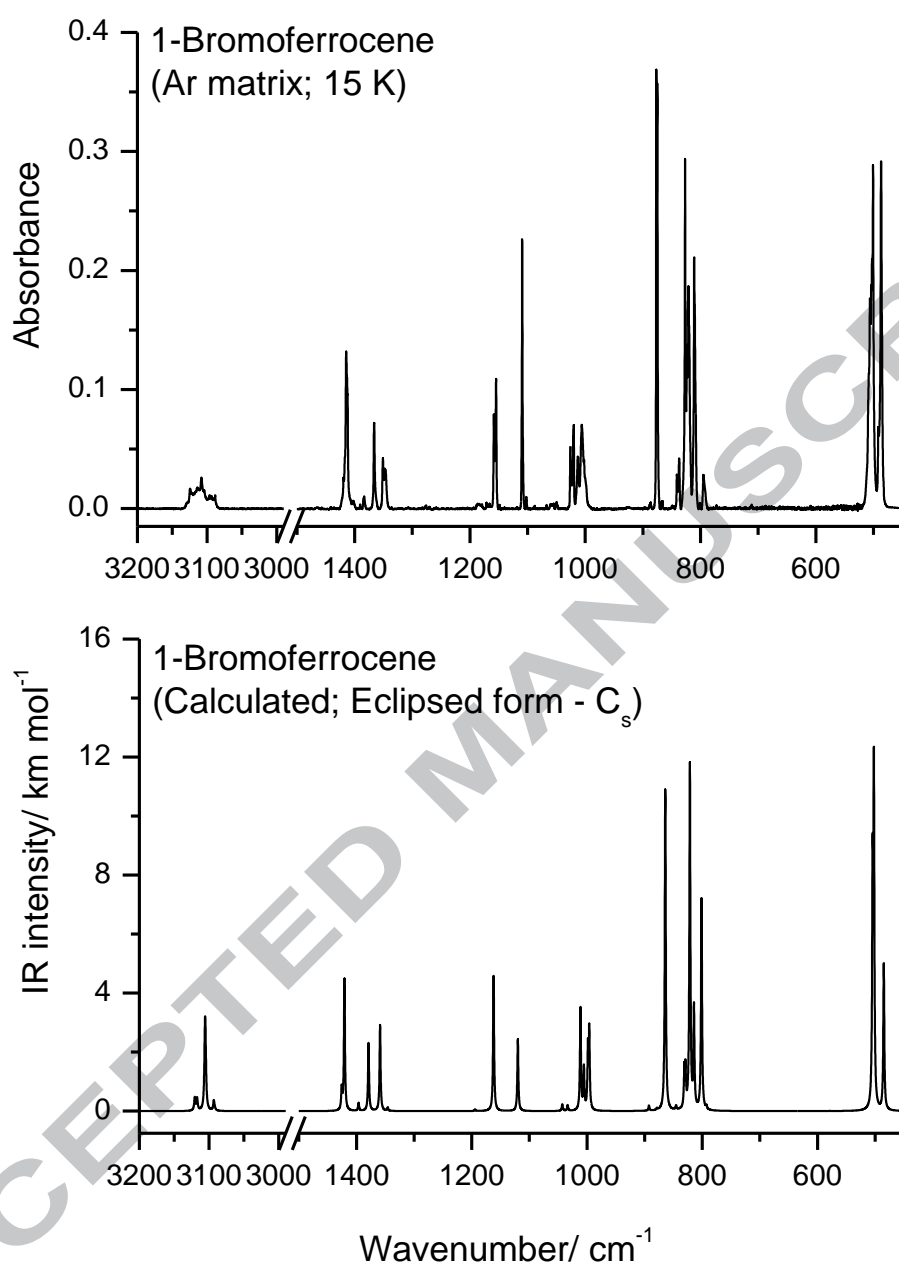


Figure 6. Observed infrared spectrum of 1-bromoferrrocene isolated in an argon matrix, at 15 K (*top*), and simulated infrared spectrum for the minimum energy conformation of the compound (eclipsed form; *bottom*).

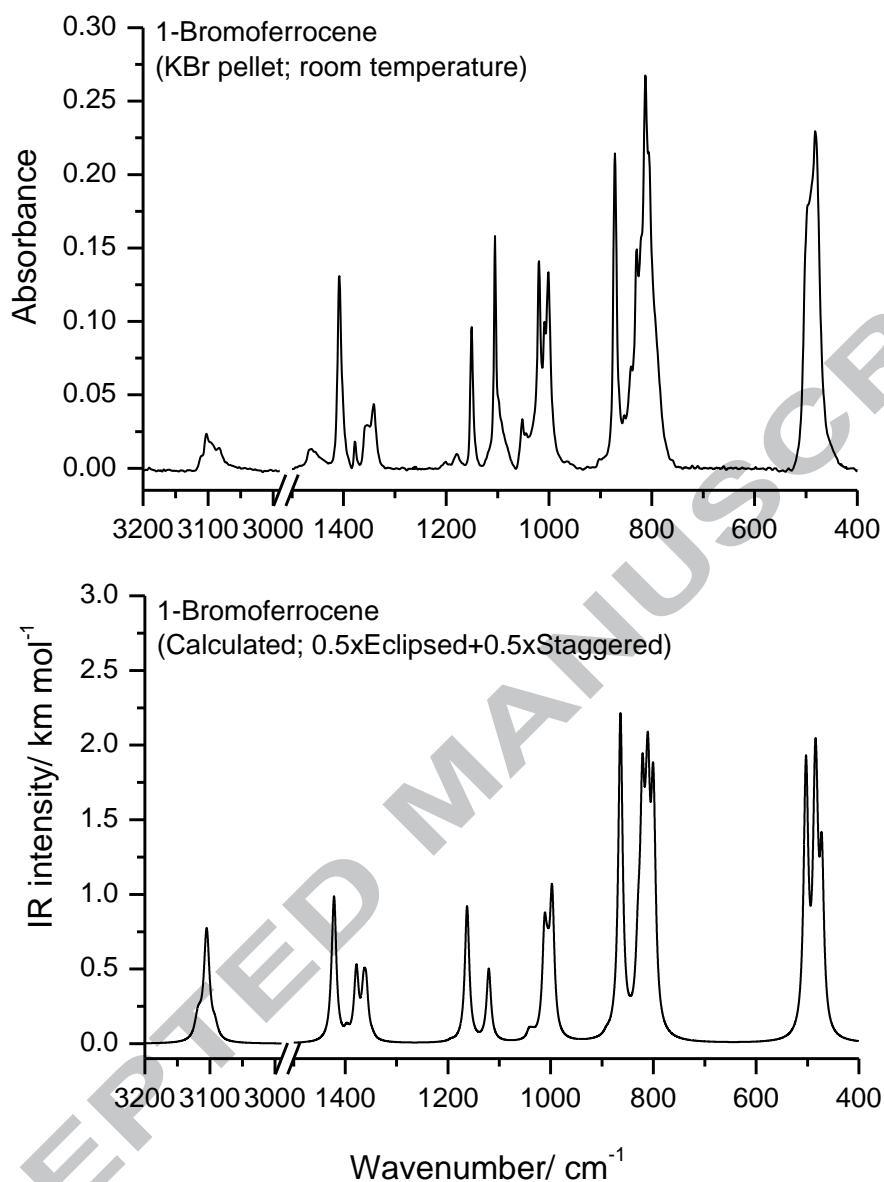


Figure 7. Observed room temperature infrared spectrum of crystalline 1-bromoferrocene in KBr pellet (*top*) and simulated infrared spectrum based on the sum of the B3LYP/LANL2DZ + cc-pVDZ calculated (scaled) spectra for the eclipsed and staggered conformations of the molecule of the compound (*bottom*). In the simulated spectrum bands were broadened by convoluting each peak with a Lorentzian function with a full width at half-maximum (FWHM) of 10 cm⁻¹. Note that the calculated intensities correspond to the area between the peaks, so that the intensities provided in Table 5 do not fit the peak intensities in the plot.

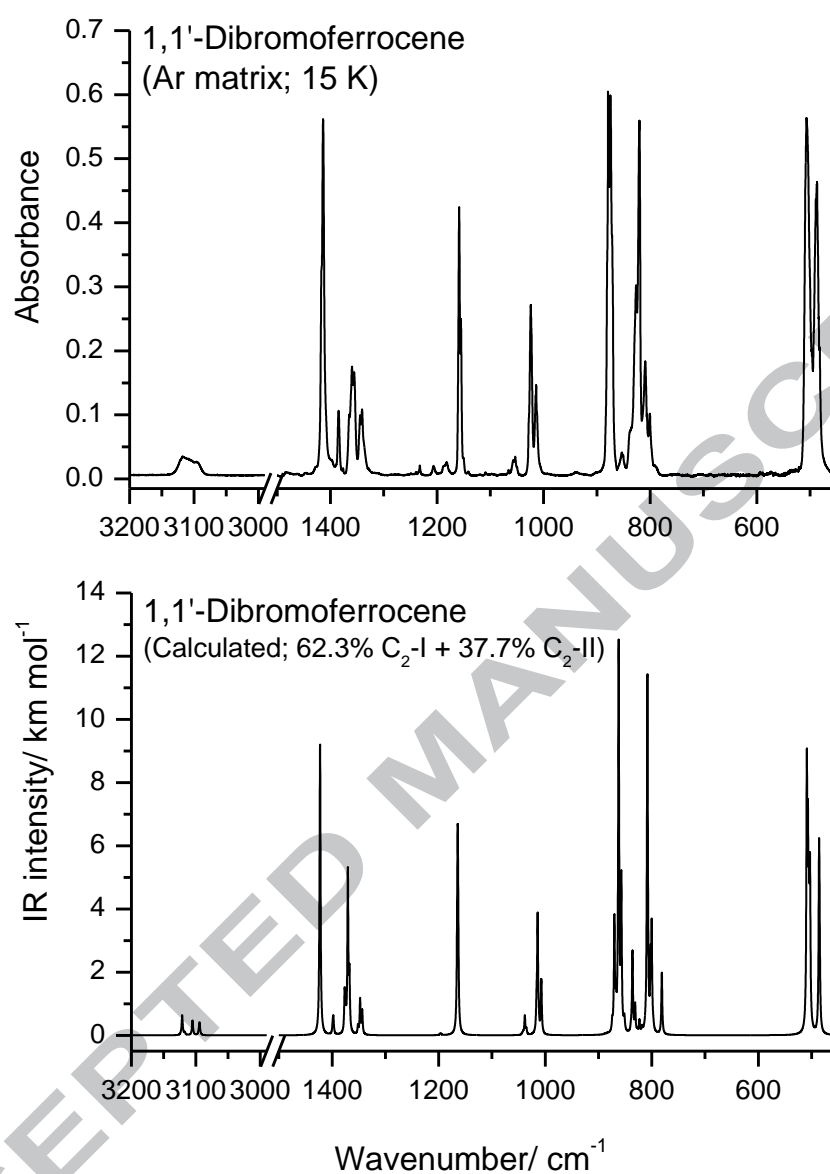


Figure 8. Observed infrared spectrum of 1,1'-dibromoferrocene isolated in an argon matrix, at 15 K (*top*), and simulated infrared spectrum constructed by adding the B3LYP/LANL2DZ + cc-pVDZ calculated infrared spectra of conformers C₂-I and C₂-II weighted by their theoretically estimated relative populations in gas phase prior to deposition (C₂-I, 62%; C₂-II, 38%) (*bottom*).

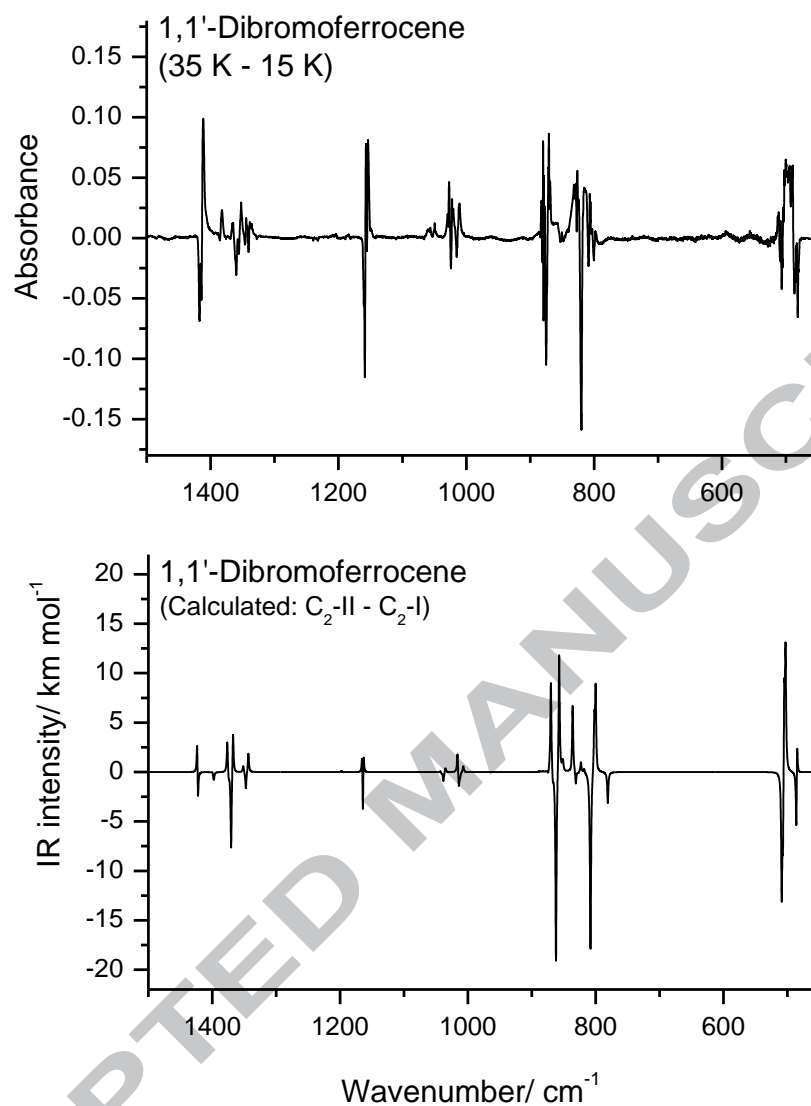


Figure 9. Observed infrared difference spectrum of 1,1'-bromoferrocene isolated in an argon matrix (spectrum obtained after warming of the matrix up to 35 K, minus spectrum of the as-deposited matrix at 15 K) (*top*), and simulated infrared difference spectrum obtained by subtracting the B3LYP/LANL2DZ + cc-pVDZ calculated spectrum of C₂-I from that of C₂-II.

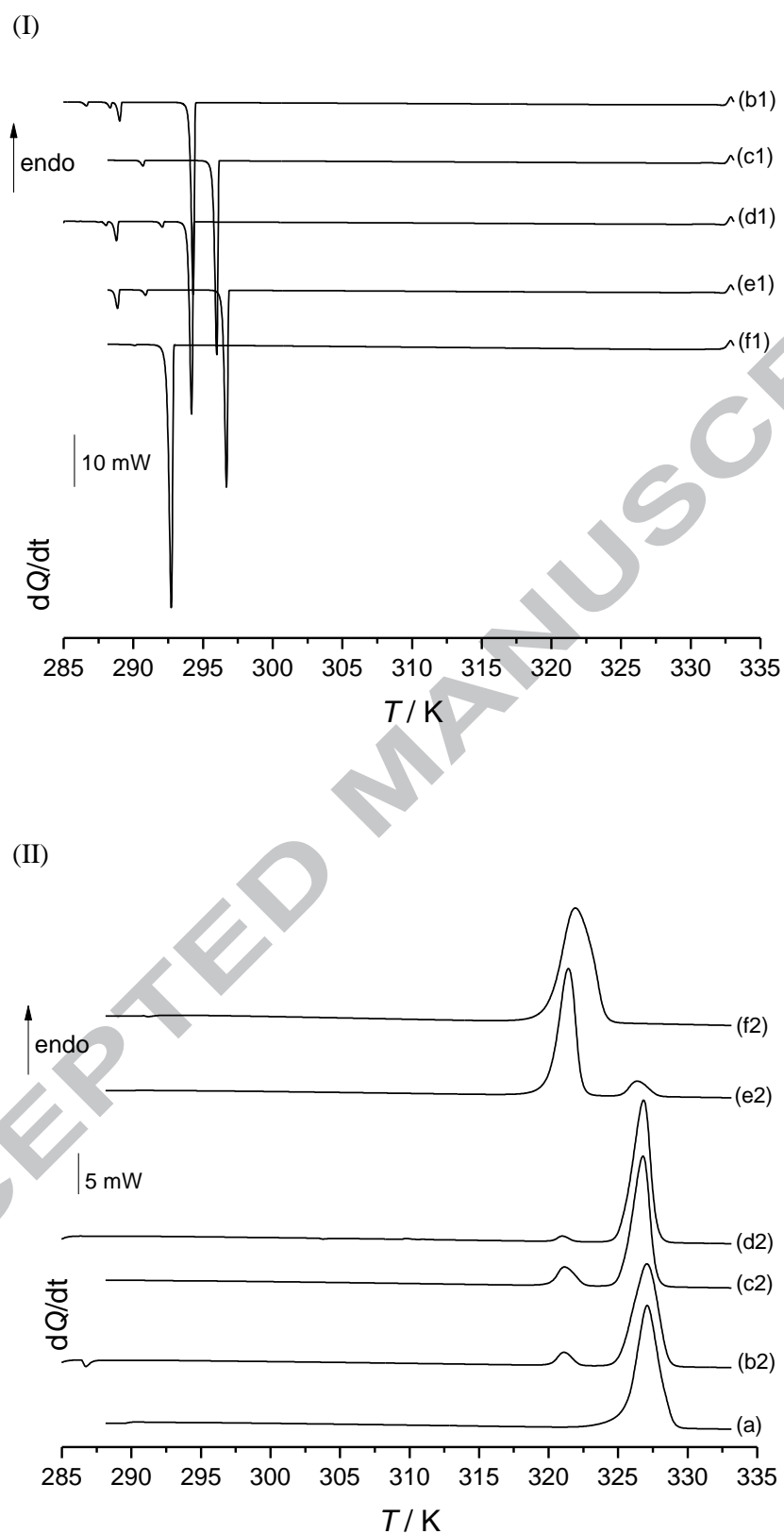


Figure 10. DSC traces of 1,1'-dibromoferrocene samples: (I) obtained from two samples in heating runs, with heating rate of 10 K min⁻¹; (a) original compound; (b2-f2) following melt crystallization at cooling rate -5 K min⁻¹; (b2-e2) $m = 2.57$ mg; (f2) $m = 3.33$ mg; (II) obtained from melt cooling; (b1-e1) $m = 2.57$ mg; (f1) $m = 3.33$ mg.

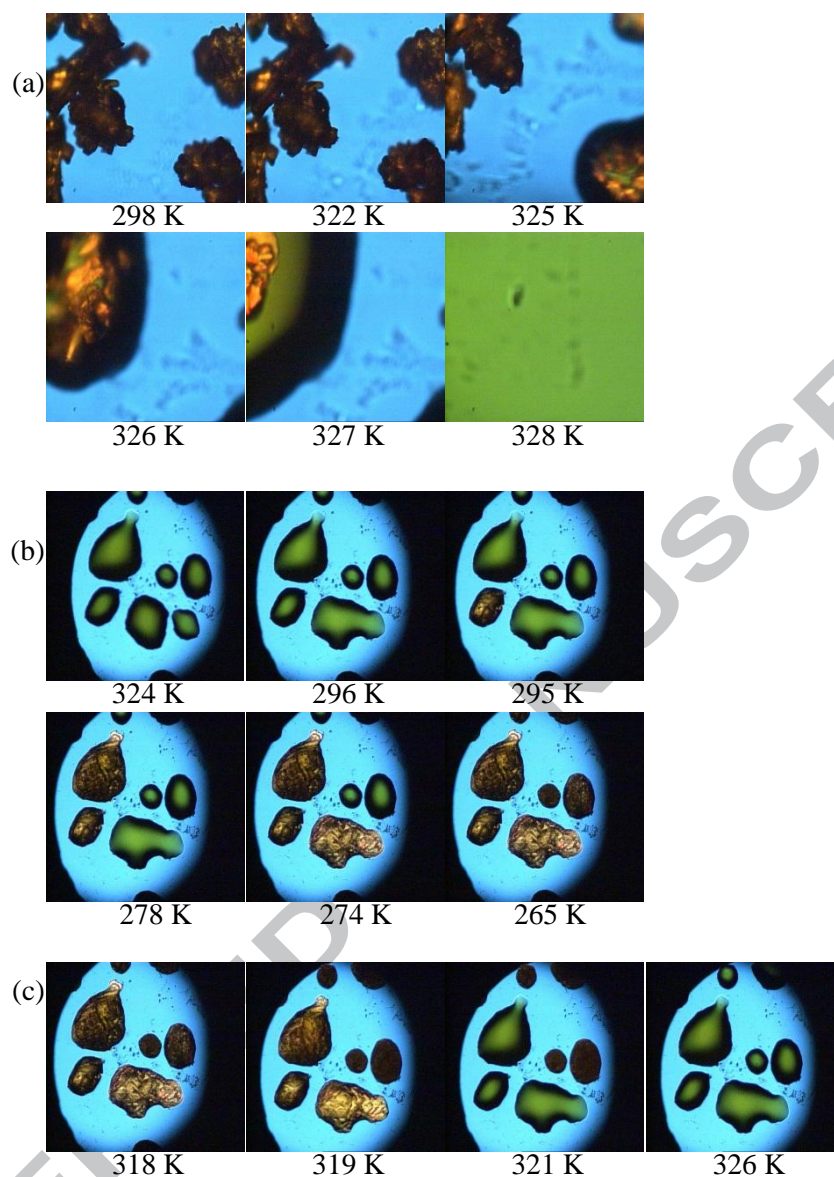


Figure 11. PLTM images of 1,1'-dibromoferrocene samples. (a) original compound; heating rate 10 K min^{-1} ; magnification $200\times$; (b) melt cooling; cooling rate -5 K min^{-1} ; (c) heating run of the molten crystallized sample; heating rate 10 K min^{-1} ; magnification $50\times$.

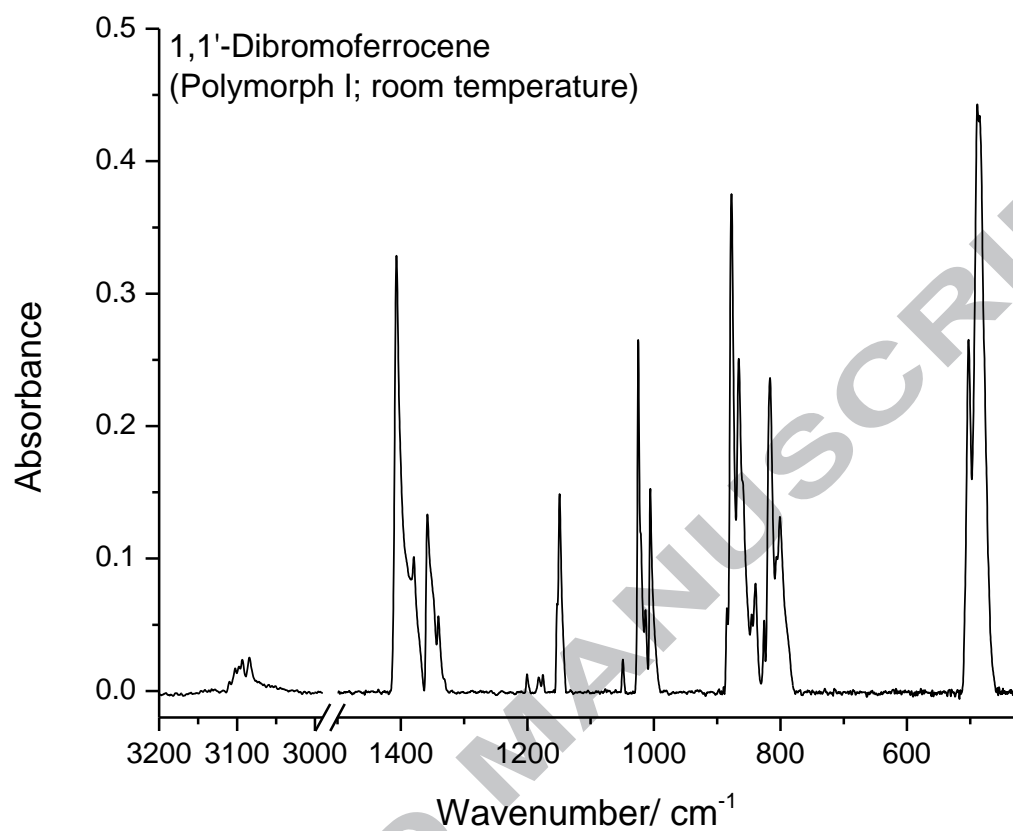


Figure 12. Observed infrared spectrum of polymorph I of 1,1'-dibromoferrocene at room temperature.

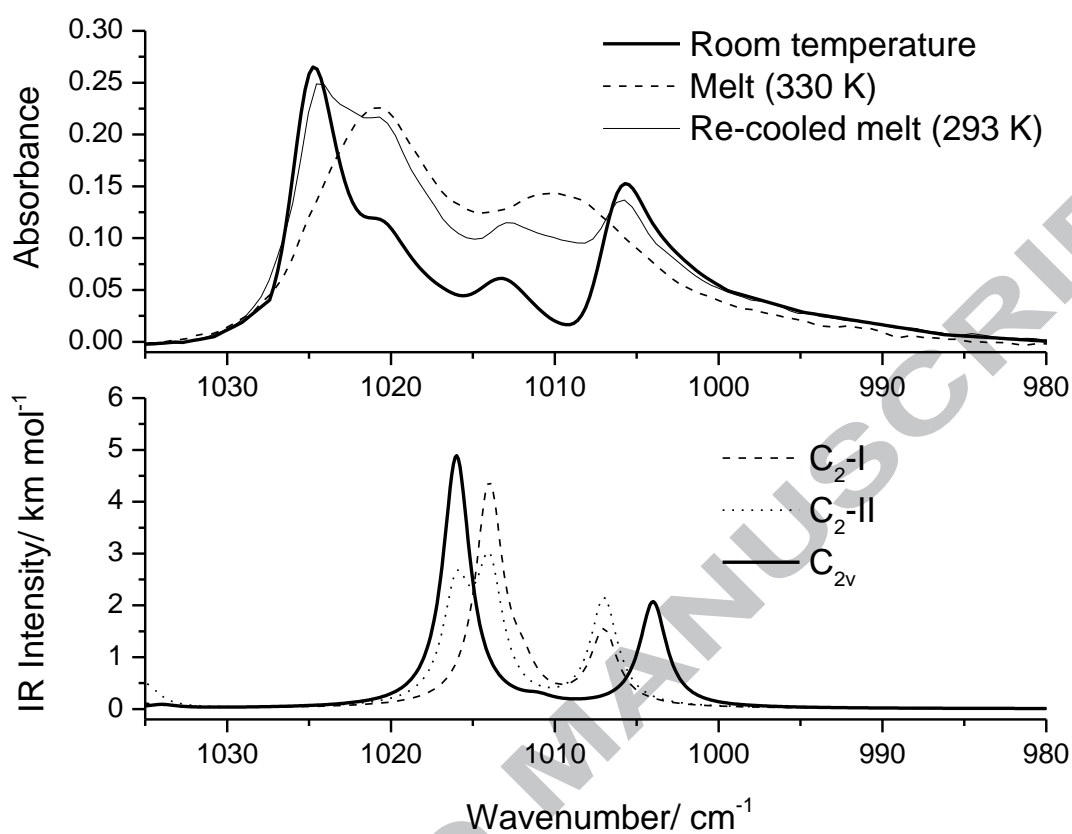


Figure 13. Experimental infrared spectra of 1,1'-dibromoferrocene in the 1035-980 cm^{-1} range at different temperatures (*top*), and calculated spectra for the $C_2\text{-I}$, $C_2\text{-II}$ and C_{2v} forms (*bottom*). According to the X-ray structure of polymorph I of the compound [57], in the room temperature crystal molecules assume the C_{2v} conformation. In the liquid phase, one can expect that the molecules assume the minimum energy conformations for the isolated molecule ($C_2\text{-I}$ and $C_2\text{-II}$). Note also that the spectrum of the re-cooled melt at 293 K reveals that the compound had not yet fully crystallized at that temperature.

Table 1: B3LYP/LANL2DZ + cc-pVDZ calculated relative energies for minima and transition state structures of ferrocene, 1-bromoferrrocene and 1,1'-dibromoferrrocene, and expected room temperature gas-phase populations (p) for the two conformers of 1,1'-dibromoferrrocene.^a

Form	Ferrocene		1-Bromoferrrocene		1,1'-Dibromoferrrocene				
	Symmetry	ΔE	Symmetry	ΔE	Symmetry	ΔE	ΔE°	ΔG	p
Staggered	D _{5d}	1.96	C _s	1.87	C ₂	1.38			
					C _{2h}	1.66			
Eclipsed	D_{5h}	0.00	C _s	0.00	C _{2v}	5.73			
					C₂-I	0.00			62.3%
					C₂-II	0.82	1.50	1.25	37.7%

^a Relative energies without (ΔE) or with ΔE° zero-point correction and Gibbs relative energies (ΔG) in kJ mol⁻¹. Calculated absolute electronic energies for the most stable form of the molecules are: ferrocene: -510.543201032 E_h; 1-bromoferrrocene: -3084.09447013 E_h; 1,1'-dibromoferrrocene: -5657.64540445 E_h. Structures in **bold** style correspond to minima.

Table 2: B3LYP/LANL2DZ + cc-pVDZ calculated geometries for minima and transition state structures of ferrocene, 1-bromoferrocene and 1,1'-dibromoferrocene, and experimental geometries for the experimentally observed forms (in gas phase).^a

Parameter ^b	Ferrocene			1-Bromoferrocene			1,1'-Dibromoferrocene				
	D_{5h}	D_{5h} ^c	D _{5d}	C_s	C_s ^d	C _s	C _{2-I}	C _{2-II}	C ₂	C _{2h}	C _{2v}
C–C	1.430	1.431(5)	1.428	1.430	1.433(1)	1.429	1.429	1.429	1.429	1.429	1.429
C–H	1.088	1.116(12)	1.088	1.088	1.08	1.088	1.087	1.087	1.087	1.087	1.088
C–Br				1.903	1.875(11)	1.903	1.902	1.901	1.902	1.902	1.896
Fe–C(Cp)	2.074	2.058(5)	2.077	2.076	2.035(16)	2.077					
Fe–C(CpBr)				2.071	2.067(25)	2.073	2.072	2.072	2.074	2.074	2.076
H-(CCC)	1.7	4.6(27)	2.0	1.7	4.6	1.9	1.7	1.7	1.8	1.7	1.1
Br-(CCC)				2.9	0.0	2.2	2.4	2.4	1.9	1.8	4.4

^a Distances in Å, angles in degrees. Structures in **bold** style correspond to minima. ^b Average values of the parameters are given in this table; the individual parameters' values can be obtained from the Cartesian coordinates of the various structures provided as Supporting Material (Table S1); Cp and CpBr designate the unsubstituted and the bromo-substituted cyclopentadienyl rings, respectively. ^c Electron diffraction data ($r_g(0) \sim r_e$, except for C–H distance which corresponds to uncorrected value extracted directly from the distance distribution curves in the electron diffraction study), with errors, in parentheses, in units of the last digit [27]. ^d Microwave spectroscopy data, with errors, in parentheses, in units of the last digit [30]; in the experimental study, the following assumptions were made: carbon rings were assumed to be planar with local C₅ local symmetry for both C and H atoms, C–H bond lengths were fixed as 1.08 Å, the H-(CCC) angle considered to be equal to 4.6°, and the Br atom to be co-planar with the carbon ring.

Table 3: B3LYP/LANL2DZ + cc-pVDZ calculated infrared spectrum for the eclipsed form of ferrocene, and experimental infrared spectrum for the compound isolated in an argon matrix (15 K).^a

Calculated (Eclipsed form; D _{5h})			Experimental (Ar matrix)	Approximate	
ν	I ^{IR}	Symmetry	ν^{IR}	I ^{IR b}	Description ^c
3114	2.1	A ₂ ''	} 3126/ 3124/ 3122/ 3118/ 3112/ 3107/ 3095/ 3090/ 3088	} 30.1	vCH <i>s</i>
3103	31.0	E ₁ '			vCH <i>as</i>
1415	3.0	E ₁ '	1415/ 1414	6.0	vCC <i>as</i>
1111	17.9	A ₂ ''	1111/ 1110	24.4	vCC [breath]
1007	40.6	E ₁ '	1007/ 1006/ 1005	34.6	δ CH <i>as</i>
840	10.4	E ₁ '	841/ 839/ 838	6.2	γ CH <i>as</i>
819	73.6	A ₂ ''	821/ 820/ 819/ 818	66.9	γ CH [umbrella]
500	47.2	E ₁ '	504/ 502	47.2	Cp-Fe [wag]
484	12.0	A ₂ ''	484/ 483	22.2	Cp-Fe [top-down]

^a Wavenumbers (ν ; in cm⁻¹) were scaled by 0.984, except for the vCH and Cp-Fe regions where scale factors of 0.957 and 1.083, respectively, were used; infrared intensities (I^{IR}) in km mol⁻¹; only infrared active bands appearing above 400 cm⁻¹ are shown (full calculated spectrum is provided in Table S2; Supporting information).

^b Experimental intensities correspond to integrated absorbances normalized so that the total experimental intensity equals the theoretically calculated one. ^c v, stretching; δ , bending; γ , out-of-plane bending; *s*, symmetric; *as*, anti-symmetric; Cp, cyclopentadienyl.

Table 4: Observed bands in the infrared spectra (3200-400 cm^{-1} range) of the monoclinic, triclinic and orthorhombic polymorphs of ferrocene, and of the amorphous state obtained from the vapour of the compound, and proposed assignments.^a

Monoclinic	Triclinic	Orthorhombic	Amorphous	Approximate Description ^b
3105/ 3094/ 3083	} 3106/ 3094/ 3082	} 3108/ 3104/ 3095 3083/ 3080	} 3110/ 3098/ 3087	} vCH <i>s</i> vCH <i>as</i>
1409/ 1402				
1352	1348	1359/ 1346	1363/ 1347	vCC <i>as</i>
1256	1256	1257/ 1253	1255	δ CH <i>s</i>
1191	1192	1194	1189	δ CH <i>as</i>
1106/1097	1106/1097	1106/ 1097	1107/ 1103	vCC [breath]
1057/1047	} 1058/1048	} 1064/ 1061/ 1058 1051/ 1047/ 1044	} 1058/1047	} γ CH <i>as</i>
1001				
895/ 881/ 865	897/ 882	902/ 897/ 887/882	} 889	} δ CCC
855/ 844	858/ 845	857/ 853/ 847/ 844		
820/ 815	820/ 816	822/ 818	821	γ CH [umbrella]
786	790	793	792	?
488	492	500	500	Cp-Fe [wag]
476	478	481	481	Cp-Fe [top-down]

^a Wavenumbers (ν ; in cm^{-1}). ^b ν , stretching; δ , bending; γ , out-of-plane bending; *s*, symmetric; *as*, anti-symmetric; Cp, cyclopentadienyl; ?, probably an overtone or combination band. In the crystalline states, degeneracies present in the isolated molecule are removed under the site symmetries and because there are more than one molecule per unit cell, so that some inactive modes for the isolated molecule become IR active in the crystals. Bulk static disorder in the amorphous state also leads to symmetry breakdown and observation of IR inactive modes for the isolated molecule. The assignments proposed here follow those presented in [50].

Table 5: B3LYP/LANL2DZ + cc-pVDZ calculated infrared spectrum for the eclipsed form of 1-bromoferrocene, and experimental infrared spectrum for the compound isolated in an argon matrix (15 K).^a

Calculated (Eclipsed-form; C _s)			Experimental (Ar matrix)	Approximate Description ^b
ν	I ^{IR}	Symmetry	ν^{IR}	
3120	1.4	A'	3128	vCH <i>s</i> (1)
3117	0.8	A'	3125/ 3121	vCH <i>s</i> (2)
3117	0.5	A''	3119/ 3117	vCH _{β} <i>as</i> (1)
3106	5.4	A'	3115/ 3113/ 3108/ 3104	vCH _{γ} <i>s</i> - vCH _{α} (2)
3105	5.5	A''		vCH _{β} <i>as</i> (2)
3105	0.9	A'		vCH _{γ} <i>s</i> (1)
3093	1.0	A''	3097/ 3094/ 3091/ 3089	vCH _{β} <i>as</i> (1)
3093	0.2	A'		vCH _{β} <i>s</i> - vCH _{α} (2)
3090	0.004	A''	n.obs.	vCH _{γ} <i>as</i> (2)
1426	1.0	A''	1419	vC _{β} C _{γ} <i>as</i> (2)
1425	1.4	A'	1417	vC _{α} C _{β} <i>s</i> - vC _{γ} C _{γ} (2)
1421	14.0	A'	1415/ 1414/ 1413/ 1412	vC _{α} C _{β} <i>s</i> - vC _{γ} C _{γ} (1)
1396	0.9	A''	1384	vC _{β} C _{γ} <i>as</i> (1)
1379	7.2	A'	1366	vC _{β} C _{γ} <i>s</i> - vC _{γ} C _{γ} (1,2)
1375	0.01	A''	1362	vC _{α} C _{β} <i>as</i> (2)
1359	9.1	A'	1351/1350/1348/1347/1346	vC _{β} C _{γ} <i>s</i> - vC _{γ} C _{γ} (1,-2)
1346	0.4	A''	1307	vC _{α} C _{β} <i>as</i> (1)
1246	0.0001	A''	n.obs.	δ CH [roll] (2)
1194	0.2	A''	n.obs.	δ CH [roll] (1)
1162	14.4	A'	1158/ 1154	vCC [breath] (1)
1120	7.7	A'	1109	vCC [breath] (2)
1043	0.7	A'	1060	δ CH _{γ} <i>s</i> (1,2)
1041	0.03	A''	1055	δ CH _{α} (2)
1034	0.6	A'	1050	δ CH _{γ} <i>s</i> (1,-2)
1011	10.9	A''	1025/ 1024/ 1022/ 1019	δ CH _{γ} <i>as</i> (1)
1005	4.4	A'	1012	δ CH _{β} <i>s</i> (1)
998	6.3	A''	1007/ 1006/ 1001/ 1000/ 999/ 998	δ CH _{γ} <i>as</i> (2)
996	8.3	A'		δ CH _{β} <i>s</i> (2)
892	0.6	A'	887	γ CH _{β} <i>s</i> - γ CH _{α} (2)
885	0.006	A''	n.obs.	γ CH _{β} <i>as</i> - γ CH _{γ} <i>as</i> (1,-2)
879	0.2	A'	877/ 875	γ CH _{β} <i>as</i> - γ CH _{γ} <i>as</i> (1,2)
864	34.2	A'	867/ 865	vCBr + δ C _{β} C _{α} C _{β}
845	0.4	A'	850	γ CH _{β} <i>s</i> - γ CH _{γ} <i>s</i> (1)
838	0.02	A''		δ C _{β} C _{γ} C _{γ} <i>as</i> (1,2)
831	3.9	A''	841/ 840	γ CH _{β} <i>as</i> + γ CH _{γ} <i>as</i> (1, -2)
829	4.0	A'	837	δ C _{β} C _{α} C _{β} (2)
821	1.2	A''	831	δ C _{β} C _{γ} C _{γ} <i>as</i> (1, -2)
821	35.7	A'	827/ 826/ 824/ 822	γ CH _{β} <i>s</i> + γ CH _{α} (2)
814	10.7	A'	821/ 820/ 819	γ CH <i>s</i> [umbrella] (1, -2)
801	22.5	A'	811/ 810/ 808	γ CH _{γ} <i>s</i> (1,2)
793	0.3	A''	794	γ CH _{β} <i>as</i> + γ CH _{γ} <i>as</i> (1, 2)
578	0.02	A'	n.obs.	τ_{ring} [puckering] (1, -2)
578	0.001	A''	n.obs.	τ_{ring} [twist] (2)
568	0.001	A'	n.obs.	τ_{ring} [puckering] (1, 2)
568	0.006	A''	n.obs.	τ_{ring} [twist] (1)
504	23.4	A''	508/ 507/ 505/ 504/ 503/ 502/ 500	Cp-Fe [wag]
502	34.7	A'		Cp-Fe [top-down C _{α} (2)/C _{γ} C _{γ} (1)]
485	15.6	A'	491/ 490/ 489/ 486/ 485	Cp-Fe [top-down C _{α} (1)/C _{γ} C _{γ} (2)]

^a Wavenumbers (ν ; in cm⁻¹) were scaled by 0.984, except for the vCH and Cp-Fe regions where scale factors of 0.957 and 1.083, respectively, were used; infrared intensities (I^{IR}) in km mol⁻¹; n.obs, not observed; only bands appearing above 400 cm⁻¹ are shown (full calculated spectrum is provided in Table S2; Supporting information).

^b ν , stretching; δ , bending; γ , out-of-plane bending; τ , torsion; *s*, symmetric; *as*, anti-symmetric; bromosubstituted and unsubstituted cyclopentadienyl (Cp) rings are designated by numbers (1) and (2), respectively; α , β and γ subscripts designate the CH group of ring (2) eclipsed with the CBr group of ring (1), and CH groups at the *ortho* and *meta* positions regarding the CBr group (or α -CH group in case of the unsubstituted ring), respectively.

Table 6: Observed infrared spectrum of crystalline 1-bromoferrocene (3200-400 cm^{-1} range; room temperature) and proposed assignments.^a

ν	Approximate Description ^b	ν	Approximate Description ^b	
3110	νCH_s (1)	1052	} $\delta\text{CH}_\gamma s$ (1,2)	
3103	νCH_s (2)			} δCH_α (2)
3096	$\nu\text{CH}_\beta as$ (1)	1045	$\delta\text{CH}_\gamma s$ (1,-2)	
3092	} $\nu\text{CH}_\gamma s - \nu\text{CH}_\alpha$ (2)	1020	} $\delta\text{CH}_\gamma as$ (1)	
		$\nu\text{CH}_\beta as$ (2)		} $\delta\text{CH}_\beta s$ (1)
		$\nu\text{CH}_\gamma s$ (1)	1008	
3083		} $\nu\text{CH}_\beta as$ (1)	1001	$\delta\text{CH}_\beta s$ (2)
	$\nu\text{CH}_\beta s - \nu\text{CH}_\alpha$ (2)		901	$\gamma\text{CH}_\beta s - \gamma\text{CH}_\alpha$ (2)
	$\nu\text{CH}_\gamma as$ (2)		871	$\nu\text{CBr} + \delta\text{C}_\beta\text{C}_\alpha\text{C}_\beta$
1462	$\nu\text{C}_\beta\text{C}_\gamma as$ (2)	853	$\gamma\text{CH}_\beta s - \gamma\text{CH}_\gamma s$ (1)	
1454	$\nu\text{C}_\alpha\text{C}_\beta s - \nu\text{C}_\gamma\text{C}_\gamma$ (2)	840	$\gamma\text{CH}_\beta as + \gamma\text{CH}_\gamma as$ (1, -2)	
1408	$\nu\text{C}_\alpha\text{C}_\beta s - \nu\text{C}_\gamma\text{C}_\gamma$ (1)	830	$\delta\text{C}_\beta\text{C}_\alpha\text{C}_\beta$ (2)	
1377	$\nu\text{C}_\beta\text{C}_\gamma as$ (1)	820	} $\delta\text{C}_\beta\text{C}_\gamma\text{C}_\gamma as$ (1, -2)	
1353	$\nu\text{C}_\beta\text{C}_\gamma s - \nu\text{C}_\gamma\text{C}_\gamma$ (1,2)			} $\gamma\text{CH}_\beta s + \gamma\text{CH}_\alpha$ (2)
	$\nu\text{C}_\alpha\text{C}_\beta as$ (2)	813	γCH_s [umbrella] (1, -2)	
1340	$\nu\text{C}_\beta\text{C}_\gamma s - \nu\text{C}_\gamma\text{C}_\gamma$ (1,-2)	806	$\gamma\text{CH}_\gamma s$ (1,2)	
1201	δCH [roll] (1)	795	$\gamma\text{CH}_\beta as + \gamma\text{CH}_\gamma as$ (1, 2)	
1150	νCC [breath] (1)	497	Cp-Fe [wag]	
1105	νCC [breath] (2)	490	Cp-Fe [top-down C_α (2)/ $\text{C}_\gamma\text{C}_\gamma$ (1)]	
		482	Cp-Fe [top-down C_α (1)/ $\text{C}_\gamma\text{C}_\gamma$ (2)]	

^a Wavenumbers (ν ; in cm^{-1}). ^b ν , stretching; δ , bending; γ , out-of-plane bending; s , symmetric; as , anti-symmetric; bromosubstituted and unsubstituted cyclopentadienyl (Cp) rings are designated by numbers (1) and (2), respectively; α , β and γ subscripts designate the CH group of ring (2) eclipsed with the CBr group of ring (1), and CH groups at the *ortho* and *meta* positions regarding the CBr group (or α -CH group in case of the unsubstituted ring), respectively.

Table 7: B3LYP/LANL2DZ + cc-pVDZ calculated infrared spectra for the two conformers of 1,1'-dibromoferrocene, and experimental infrared spectrum for the compound isolated in an argon matrix (15 K).^a

Calculated					Experimental (Ar matrix)		Approximate Description ^b
C ₂ -I ν	I ^{IR}	C ₂ -II ν	I ^{IR}	Sym.	ν^{IR} (C ₂ -I)	ν^{IR} (C ₂ -II)	
3121	0.2	3121	1.9	A	} 3117		vCH <i>s</i>
3121	1.4	3121	0.7	B			vCH <i>s</i>
3117	0.3	3117	0.1	A	} 3109		vCH _{β} <i>as</i>
3117	0.04	3117	0.04	B			vCH _{β} <i>as</i>
3105	0.9	3105	1.3	B	} 3103		vCH _{β} <i>s</i> – vCH _{γ} <i>s</i>
3105	0.1	3105	0.9	A			vCH _{β} <i>s</i> – vCH _{γ} <i>s</i>
3095	0.03	3094	0.6	B	} 3095		vCH _{γ} <i>as</i>
3094	1.2	3095	1.1	A			vCH _{γ} <i>as</i>
1422	29.0	1422	14.7	B	} 1417/ 1414	} 1412	vC _{α} C _{β} <i>s</i> – vC _{γ} C _{γ}
1422	2.4	1423	17.3	A			vC _{α} C _{β} <i>s</i> – vC _{γ} C _{γ}
1398	1.3	1398	0.7	B	} 1385	} 1382	vC _{β} C _{γ} <i>as</i>
1397	2.1	1399	0.3	A			vC _{β} C _{γ} <i>as</i>
1374	2.7	1367	10.4	A	1361	1352	vC _{β} C _{γ} <i>s</i> – vC _{γ} C _{γ}
1370	25.6	1376	14.2	B	1360/ 1356	1365	vC _{β} C _{γ} <i>s</i> – vC _{γ} C _{γ}
1347	5.6	1343	2.2	B	} 1340	1335	vC _{α} C _{β} <i>as</i>
1344	0.1	1351	6.1	A			vC _{α} C _{β} <i>as</i>
1196	0.01	1196	0.3	B	} 1207/ 1205	} 1209/ 1204	δ CH [roll]
1195	0.2	1197	0.1	A			δ CH [roll]
1164	24.3	1165	12.3	B	1159	1158	vCC [breath]
1163	2.3	1163	15.0	A	1155	1154	vCC [breath]
1041	0.4	1035	0.4	A	1054	1050	δ CH _{γ} <i>s</i>
1038	3.1	1043	1.5	B	1053	1057	δ CH _{γ} <i>s</i>
1014	13.5	1016	6.7	A	1024	1027	δ CH _{β} <i>as</i> – δ CH _{γ} <i>as</i>
1012	1.5	1014	8.0	B	1023	1022	δ CH _{β} <i>as</i> – δ CH _{γ} <i>as</i>
1007	4.6	1006	6.5	B	} 1015/ 1014	} 1012/ 1010	δ CH _{β} <i>s</i>
1004	0.1	1007	0.03	A			δ CH _{β} <i>s</i>
875	0.01	888	0.3	A	n.obs.	n.obs.	γ CH _{γ} <i>as</i>
874	1.5	883	0.3	B	n.obs.	n.obs.	γ CH _{γ} <i>as</i>
867	3.9	857	29.3	A	881	872/ 871	vCBr + δ C _{β} C _{α} C _{β}
862	61.8	870	39.2	B	879/ 878/ 875	880/ 879/ 877	vCBr + δ C _{β} C _{α} C _{β}
839	0.5	851	1.5	B	n.obs.	} 868	γ CH _{β} <i>s</i> – γ CH _{γ} <i>s</i>
838	0.6	852	2.6	A	n.obs.		γ CH _{β} <i>s</i> – γ CH _{γ} <i>s</i>
831	4.4	820	15.9	B	845	826	δ C _{β} C _{γ} C _{γ} <i>as</i> ^c
827	0.5	836	0.01	A	n.obs.	n.obs.	δ C _{β} C _{γ} C _{γ} <i>as</i>
809	4.7	802	1.3	A	} 820	n.obs.	γ CH _{β} <i>as</i>
808	54.7	823	21.3	B			γ CH <i>s</i> [umbrella]
797	0.7	818	3.2	A	809	824	γ CH <i>s</i> [umbrella]
781	9.8	800	25.9	B	801	811	γ CH _{β} <i>as</i> ^d
577	0.001	578	0.02	B	} 594/ 590		τ_{ring} [puckering]
575	0.006	568	0.01	A			τ_{ring} [puckering]
570	0.01	566	0.02	B			τ_{ring} [twist]
567	0.002	576	0.02	A			τ_{ring} [twist]
509	39.0	505	28.5	B	509	} 500-496	Cp-Fe [top-down C _{γ} /C _{γ}]
507	24.9	503	38.1	A	506		Cp-Fe [wag]
486	25.4	485	18.3	B	487	489	Cp-Fe [top-down C _{α} /C _{α}] ^e

^a Wavenumbers (ν ; in cm⁻¹) were scaled by 0.984, except for the vCH and Cp-Fe regions where scale factors of 0.957 and 1.083, respectively, were used; infrared intensities (I^{IR}) in km mol⁻¹; n.obs., not observed; only bands appearing above 400 cm⁻¹ are shown (full calculated spectrum is provided in Table S2; Supporting information).

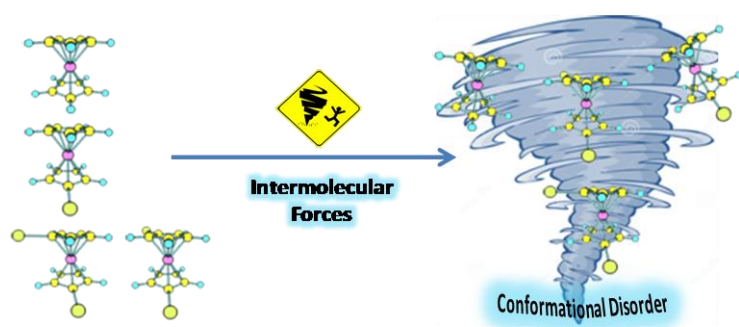
^b ν , stretching; δ , bending; γ , out-of-plane bending; τ , torsion; *s*, symmetric; *as*, anti-symmetric; β and γ subscripts designate the CH groups in each ring at the *ortho* and *meta* positions regarding the CBr group, respectively; C _{α} corresponds to the carbon atom of the CBr groups. ^c In form C₂-II, also with a significant contribution from γ CH _{β} *as*. ^d In form C₂-II, also with significant contribution of γ CH _{γ} *as*. ^e In form C₂-II, Cp-Fe [top-down C _{β} /C _{β}].

Table 8: Observed infrared spectrum of polymorph I of 1,1'-dibromoferrocene (3200-400 cm^{-1} range; room temperature) and proposed assignments.^a

	Approximate Description ^b		Approximate Description ^b
3110	$\nu\text{CH } s$	1013/ 1005	$\delta\text{CH}_\beta s$
3102	$\nu\text{CH}_\beta as$	884	$\gamma\text{CH}_\gamma as$
3097/ 3093	$\nu\text{CH}_\beta s - \nu\text{CH}_\gamma s$	877	$\nu\text{CBr} + \delta\text{C}_\beta\text{C}_\alpha\text{C}_\beta$
3084	$\nu\text{CH}_\gamma as$	865/ 858	$\gamma\text{CH}_\beta s - \gamma\text{CH}_\gamma s$
1407	$\nu\text{C}_\alpha\text{C}_\beta s - \nu\text{C}_\gamma\text{C}_\gamma$	845/ 839	$\delta\text{C}_\beta\text{C}_\gamma\text{C}_\gamma as; \gamma\text{CH}_\beta as.$
1379	$\nu\text{C}_\beta\text{C}_\gamma as$	852	$\gamma\text{CH}_\beta as$
1358/ 1352	$\nu\text{C}_\beta\text{C}_\gamma s - \nu\text{C}_\gamma\text{C}_\gamma$	816/ 809	$\gamma\text{CH } s$ [umbrella]
1340	$\nu\text{C}_\alpha\text{C}_\beta as$	801	$\gamma\text{CH}_\beta as; \gamma\text{CH}_\gamma as.$
1201	δCH [roll]	503	Cp-Fe [top-down $\text{C}_\gamma/\text{C}_\gamma$]
1152/ 1149	νCC [breath]	489	Cp-Fe [wag]
1049	$\delta\text{CH}_\gamma s$	485	Cp-Fe [top-down $\text{C}_\alpha/\text{C}_\alpha; \text{C}_\beta/\text{C}_\beta$]
1024/ 1023	$\delta\text{CH}_\beta as - \delta\text{CH}_\gamma as$		

^a Wavenumbers (ν ; in cm^{-1}). ^b ν , stretching; δ , bending; γ , out-of-plane bending; s , symmetric; as , anti-symmetric; β and γ subscripts designate the CH groups in each ring at the *ortho* and *meta* positions regarding the CBr group, respectively; C_α corresponds to the carbon atom of the CBr groups.

Graphical Abstract



ACCEPTED MANUSCRIPT

Highlights

- Potential energy landscapes were obtained theoretically for ferrocene, 1-bromoferrocene and 1,1'-dibromoferrocene.
- The conformational preferences for the isolated molecules were confirmed by matrix isolation IR spectroscopy.
- Intermolecularly-induced conformational disorder in the different polymorphs of the compounds was evaluated.
- A new polymorph of 1,1'-dibromoferrocene was discovered.